View metadata, citation and similar papers at core.ac.uk

brought to you by CORE

provided by UNT Digital Library

SANDIA REPORT
SAND2008-7203
Unlimited Release
Printed November 2008

The Sandia MEMS Passive Shock Sensor: FY08 Design Summary

Jonathan W. Wittwer, Michael S. Baker, John A. Mitchell, David S. Epp, Rebecca C. Clemens, Matthew R. Brake, Jeremy A. Walraven.

Prepared by
Sandia National Laboratories
Albuquerque, New Mexico 87185 and Livermore, California 94550

Sandia is a multiprogram laboratory operated by Sandia Corporation,
a Lockheed Martin Company, for the United States Department of Energy's
National Nuclear Security Administration under Contract DE-AC04-94AL85000.

Approved for public release; further dissemination unlimited.

Issued by Sandia National Laboratories, operated for the United States Department of Energy by Sandia Corporation.

NOTICE: This report was prepared as an account of work sponsored by an agency of the United States Government. Neither the United States Government, nor any agency thereof, nor any of their employees, nor any of their contractors, subcontractors, or their employees, make any warranty, express or implied, or assume any legal liability or responsibility for the accuracy, completeness, or usefulness of any information, apparatus, product, or process disclosed, or represent that its use would not infringe privately owned rights. Reference herein to any specific commercial product, process, or service by trade name, trademark, manufacturer, or otherwise, does not necessarily constitute or imply its endorsement, recommendation, or favoring by the United States Government, any agency thereof, or any of their contractors or subcontractors. The views and opinions expressed herein do not necessarily state or reflect those of the United States Government, any agency thereof, or any of their contractors.

Printed in the United States of America. This report has been reproduced directly from the best available copy.

Available to DOE and DOE contractors from
U.S. Department of Energy
Office of Scientific and Technical Information
P.O. Box 62
Oak Ridge, TN 37831

Telephone: (865) 576-8401
Facsimile: (865) 576-5728
E-Mail: reports@adonis.osti.gov
Online ordering: http://www.osti.gov/bridge

Available to the public from
U.S. Department of Commerce
National Technical Information Service
5285 Port Royal Rd.
Springfield, VA 22161

Telephone: (800) 553-6847
Facsimile: (703) 605-6900
E-Mail: orders@ntis.fedworld.gov
Online order: http://www.ntis.gov/help/ordermethods.asp?loc=7-4-0#online

SAND2008-7203
Unlimited Release
Printed November 2008

The Sandia MEMS Passive Shock Sensor: FY08 Design Summary

Jonathan W. Wittwer, Michael S. Baker
MEMS Technologies Department

John A. Mitchell, Rebecca C. Clemens
Electromechanical Engineering Department

David S. Epp, Matthew R. Brake
Applied Mechanics Department

Jeremy A. Walraven
Failure Analysis Department

Sandia National Laboratories
P.O. Box 5800
Albuquerque, New Mexico 87185-MS1069

Abstract

This report summarizes design and modeling activities for the MEMS passive shock sensor. It provides a description of past design revisions, including the purposes and major differences between design revisions but with a focus on Revisions 4 through 7 and the work performed in fiscal year 2008 (FY08). This report is a reference for comparing different designs; it summarizes design parameters and analysis results, and identifies test structures. It also highlights some of the changes and or additions to models previously documented [Mitchell et al. 2006, Mitchell et al. 2008] such as the way uncertainty thresholds are analyzed and reported. It also includes dynamic simulation results used to investigate how positioning of hard stops may reduce vibration sensitivity.

Acknowledgments

The authors gratefully acknowledge funding and support from the Embedded Evaluation program run by Bob Paulsen and Paul Yoon, the Campaign 6 program run by T. Y. Chu, the Campaign 5 program run by Davina Kwon, the DSW Campaign run by Mike Sjulin and Russ Miller, and the overall support and guidance of Mary Gonzales. Without this support the accomplishments documented here would have not been possible. Finally, special thanks go to Patricia Oliver for helping to create the form and legibility of the report.

Contents

1. Introduction ... 9
   1.1 Design Revisions ... 9
   1.2 Fault Tree Analysis ... 17
   1.3 Test Structures ... 18
2. Modeling ... 19
   2.1 Convergence Issues ... 21
   2.2 Bi-stable Mechanism Design Parameters ... 22
   2.3 Optimization of the Bi-stable Mechanisms ... 23
   2.4 Effect of Temperature on the Set Point ... 25
   2.5 Positioning the Hard Stop to Reduce Vibration Sensitivity ... 26
   2.6 Dynamic Simulations ... 28
   2.7 Model Validation ... 31
3. Conclusion ... 33
4. Future Work ... 35
5. References ... 37

Appendix A: Reference Information and Revision Notes for Revisions 4, 5, 6, and 7 ... 39

Appendix B: SCBM ANSYS Model ... 57

Figures

Figure 1. Timeline of Shock Switch Design Submissions. ... 10
Figure 2. AutoCAD Layout for Revision 2. ... 11
Figure 3. AutoCAD Layout of Revision 4 (half module). ... 12
Figure 4. AutoCAD layout of Revision 5. ... 14
Figure 5. AutoCAD layout for Revision 6. ... 15
Figure 6. AutoCAD layout for Revision 7. ... 16
Figure 7. Design parameters used in J-series models; note this particular device has 2 mass rows. ... 20
Figure 8. Design parameters for the bi-stable mechanisms. ... 22
Figure 9. Model results showing Fmin vs. edge bias for the J4D design. ... 24
Figure 10. Example of the Monte Carlo Simulation results for the Revision 7 1F design. ... 25
Figure 11. Curves showing sensitivity of Fmin to massMidWith. ... 25
Figure 12. Effect of temperature on the set point (J4C), assuming a rigid substrate. ... 26
Figure 13. Schematic showing the hard stop position relative to the mass. ... 27
Figure 14. Force vs. displacement showing hard stop location. ... 27
Figure 15. Schematics showing the as-drawn contact gap (dgap), latch distance (dlatch), actuator-to-contact spacing (dA-C), and actuator-to-mechanism spacing (dA-M). ... 28
Figure 16. 500 g's 1000 Hz WAVSYN pulse with 101 half sines ... 29

Figure 17. Model results for device J4A in response to WAVSYN inputs, showing the amplitude at which the switch closes. 29
Figure 18. Hard stop at 12 μm (the nominal design). 30
Figure 19. Hard stop at 10.9 μm, conservative distance from SSP. 30
Figure 20. Hard stop at 10.6 μm, almost touching at SSP. 30
Figure 21. Hard stop at 10.0 μm, preloaded against the hard stop. 31

Tables

Table 1. Summary of Model Results for Revision 4 13
Table 2. Summary of Model Results for Revision 7 17
Table 3. Range of Set Points for Shock Switches Using Different Revision 7 Spring Designs... 21
Table 4. Summary of Spring Parameters for Different Designs 23
Table 5. Comparison of Measured and Modeled Results for Revision 4 Shock Thresholds 32
Table 6. Comparison of Average Measured Resonant Frequencies to Modeled Results 32

Acronyms and Abbreviations

EE	Embedded evaluation
FEA	Finite element analysis
FMEA	Failure mode and effects analysis
FSP	First stable position
IFM	Interfacial force microscopy
LCC	Leadless chip carrier
LDV	Laser Doppler velocimeter
LSS	Lean six sigma
MEMS	Micro-electro-mechanical systems
MESO	Middle or intermediate size
PCB	Printed circuit board
SCBM	Stress-compensated bi-stable mechanism
SEM	Scanning electron microscopy
SNL	Sandia National Laboratories
SSP	Second stable position
SUMMiT V™	Sandia ultra-planar, multi-level MEMS technology 5
TRL	Technology readiness level
WETL	Weapons Evaluation Test Laboratory

1. Introduction

The MEMS passive shock sensor is a threshold acceleration sensor that latches an electrical contact into a closed position when it detects acceleration above its designed set point. The detection of an acceleration or shock event is done without any applied power, and power is required only to measure the open or closed state of the switch, or to reset the switch for continued sensing. A detailed description of the device, as well as information on the design, modeling, packaging, and testing is given in references [Mitchell et al. 2006, Wittwer et al. 2008, Mitchell et al. 2008]. The present report provides an overview of the different design submissions and documents the design and analysis work completed in fiscal year 2008.

1.1 Design Revisions

1.1.1 Timeline

The MEMS passive shock sensor is fabricated using the SUMMiT V™ surface micromachining process, where the typical die size is about 6×3mm (a design area of 6.34 × 2.82 mm). Normally, we use the standard SAMPLES process; but, for two different design submissions (Revision 3 and Revision 7) we used a modified SUMMiT V process described in more detail later. Figure 1 shows a timeline of the different design submissions with some of the key features and changes noted.

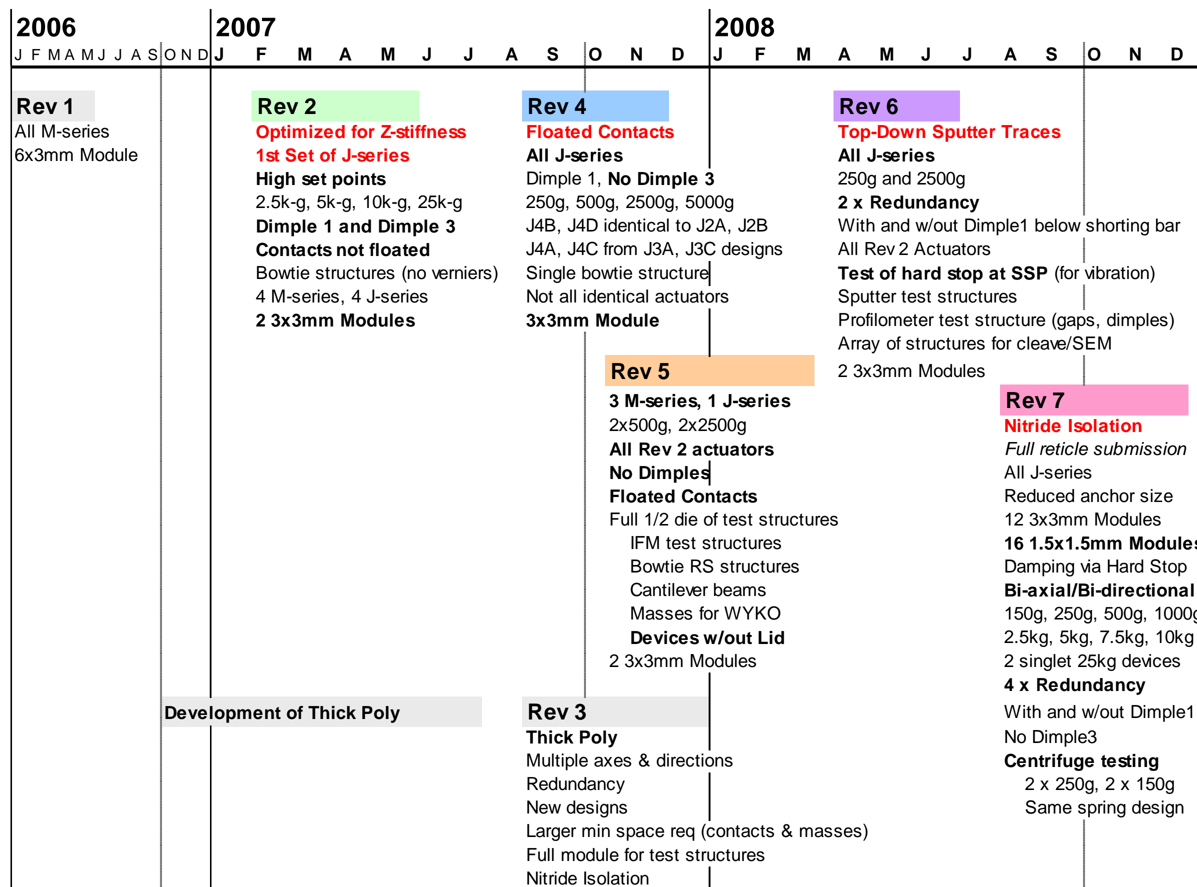

Figure 1. Timeline of Shock Switch Design Submissions.

1.1.2 Revision 1

Our first design submission was submitted in January of 2006. The design and experimental results from 2006 were included in [Mitchell et al. 2006] and later summarized and published in a conference paper in 2008 [Wittwer et al. 2008]. These references explain the basic behavior of the MEMS shock switch and describe actuator operation, the latching contacts, and the metallization process used to obtain metal-to-metal contact. They also include initial experimental results from centrifuge and hammer-strike tests as well as resonant frequency measurements.

1.1.3 Revision 2

The layout for Revision 2 is shown in Figure 2.

Reticle Set: RS630
Date Submitted: 2/19/2007 (checkplots arrive)
Date Completed: 5/18/2007 (out of fab)

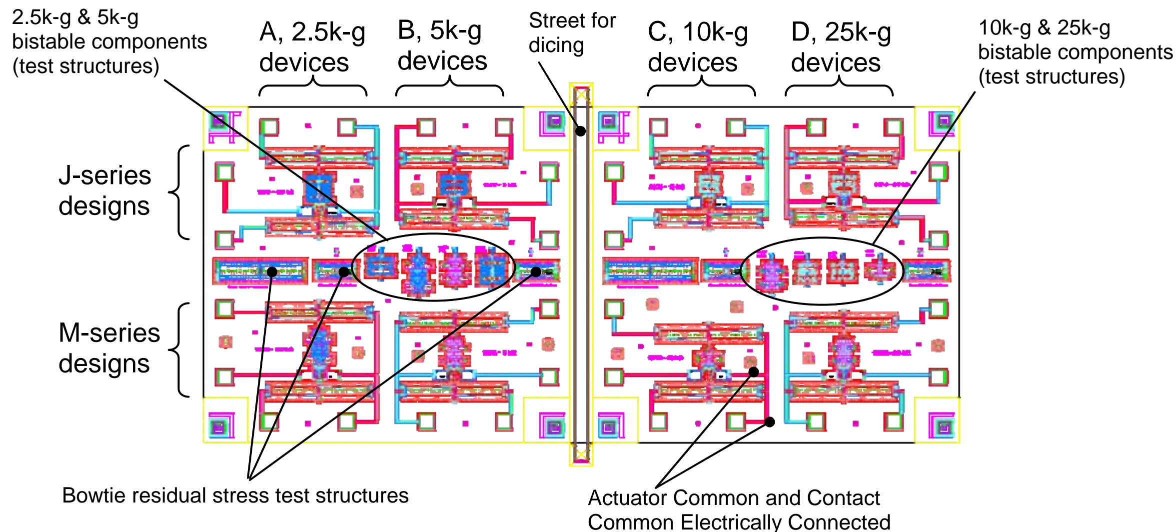

Figure 2. AutoCAD Layout for Revision 2.

Beginning with Revision 2, submitted February 2007, the module was divided into two separate 3×3mm die. The four main advantages of this approach were (1) a smaller possible overall package size, (2) less sensitivity to temperature and package-induced stresses, (3) a higher maximum shock survivability and (4) a more manageable number of bond pads. We also introduced a new spring/mass design in Revision 2, known as the J-series, to reduce the sensitivity of the device to residual stresses resulting from fabrication, packaging, and temperature changes. An extensive amount of modeling and analysis took place prior to Revision 2 to optimize the mechanisms for robustness to edge bias variation and residual stress, as well as less sensitivity to off-axis acceleration. The modeling, analysis, packaging, and testing of Revision 2 is discussed in detail in the FY07 report [Mitchell et al. 2008].

One change in Revision 2, which turned out to cause significant problems, was the addition of dimples on the mechanism. These dimples were included to prevent the device from being "welded" to the substrate during the metallization process, as well as a way to prevent the device from deflecting too far out-of-plane. Unfortunately, the dimples were the likely cause of a new failure mode – sliding friction due to closure of the dimple gap. While several factors are likely contributors to the gap closure failure, detailed analysis [Walraven et al. 2008] has shown that the gap spacing fabricated was smaller than the design specification. Overall, the gap closure was most likely a result of a combination of factors including gap spacing (fabrication out of spec), deflection of the device out-of-plane either before or during a shock event, and possibly bowing of the mass structure due to stress gradient through the mass thickness. This failure mode was identified in time to remove the Dimple 3 layer from Revision 4 designs (by skipping that step in the process), but not in time to remove Dimple 1. Although the gap closure failure was not observed in Revision 4, the advantages and disadvantages of including Dimple 1 are still questionable. For this reason, Revision 6 and Revision 7 have some devices with Dimple 1 and some without in order to mitigate risk.

Another failure mode was observed with Revision 2 parts: a silicon-to-silicon shorting/fusing issue that results when the contact Common and actuator Common are electrically connected

(see Figure 2 and reference [Mitchell et al. 2008]). This results in a failure to latch contacts into place. This is most likely due to bleeding of some actuator current through the short thereby reducing the actuator stroke and ultimately not moving the contacts far enough to latch into position.

1.1.4 Revision 3

A major effort was made by the MEMS fabrication process development team starting in the fall/winter of 2006 to develop a “thick poly” process – a modification of the SUMMiT V process with the Poly12 and Poly3 layers designed to be twice as thick as those in the standard process. This project was started based on the need for devices with a higher out-of-plane stiffness. Because of the shorting/fusing problem, a nitride isolation layer was added to the process to electrically isolate the contacts and the actuators. The thicker polysilicon resulted in different space rules, so the latching contacts have different spacing than in other designs. The actuators were also redesigned to make up for the additional required displacement.

The thicker polysilicon proved to be a difficult process change that resulted in unforeseen problems (see the failure analysis report [Walraven et al. 2008]). However, we were able to qualitatively test the strength of the nitride isolation layer, which became a major focus of Revision 7.

1.1.5 Revision 4

The layout for Revision 4 is shown in Figure 3.

Reticle Set: RS661
Date Submitted: 8/14/07 (Check plots arrive)
Date Completed: 11/6/07 (Release request)

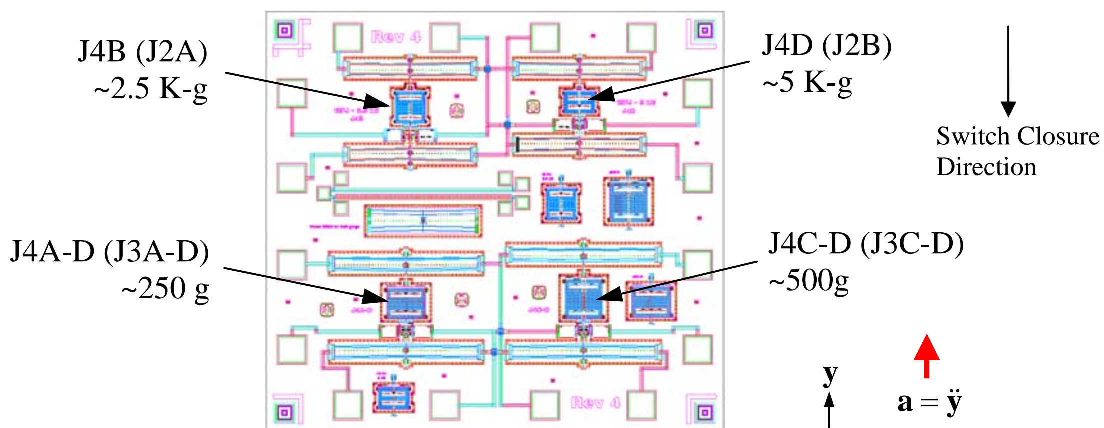

Figure 3. AutoCAD Layout of Revision 4 (half module).

The Revision 4 design submission was a result of an unexpected opportunity to use half of an unused module on the August SUMMiT V SAMPLES run, with only 2 weeks to complete the

design. The Revision 2 parts had not been shock-tested yet, but the shorting/fusing problem with the actuator and contacts was known. The main change in Revision 4 was to float the contacts so that under correct operation, current would not flow through the actuator into the electrical contact. Revision 4 was actually submitted a few days before the Revision 3 design. There was very little time for the Revision 4 submission, so 2 devices from Revision 2, and 2 devices from Revision 3 were submitted -- all with the J-series spring/mass structure. Two of the devices came directly from Revision 3. The Revision 3 actuators are different from the Revision 2 actuators and spacing in the latching contacts is also different from those in Revision 2 devices. These differences in actuators made testing more difficult, so in later revisions (Revision 5, 6, and 7), s2 actuators were used for all devices. Finally, it is noted that each device has two actuators: an open actuator and a close actuator. It is also very convenient that the open and close actuators be identical and that was true for all devices on Revision 4. Apologies if the reader is confused at this point.

Table 1 summarizes model results for the Revision 4 designs. The model is described in subsequent sections including an explanation of the uncertainty analysis. Additional details, data, and notes pertaining to Revision 4 are included in Appendix A, Section A.1..

Table 1. Summary of Model Results for Revision 4

Results from Monte Carlo Simulation

	Mass	Mean Force	Accel	Uncertainty	
Device	mg	uN	g's	Q(0.025)	Q(0.975)
J4A	4.570E-04	-1.721	384	329	406
J4C	6.130E-04	-4.777	794	688	843
J4B	4.100E-04	-12.343	3069	2517	3327
J4D	1.970E-04	-8.349	4320	1638	5342

1.1.6 Revision 5

The layout for Revision 5 is shown in Figure 4.

Reticle Set: RS676
Date Submitted: 10/17/07 (Date of final DWG File)
Date Completed: 3/11/08 (Release request)

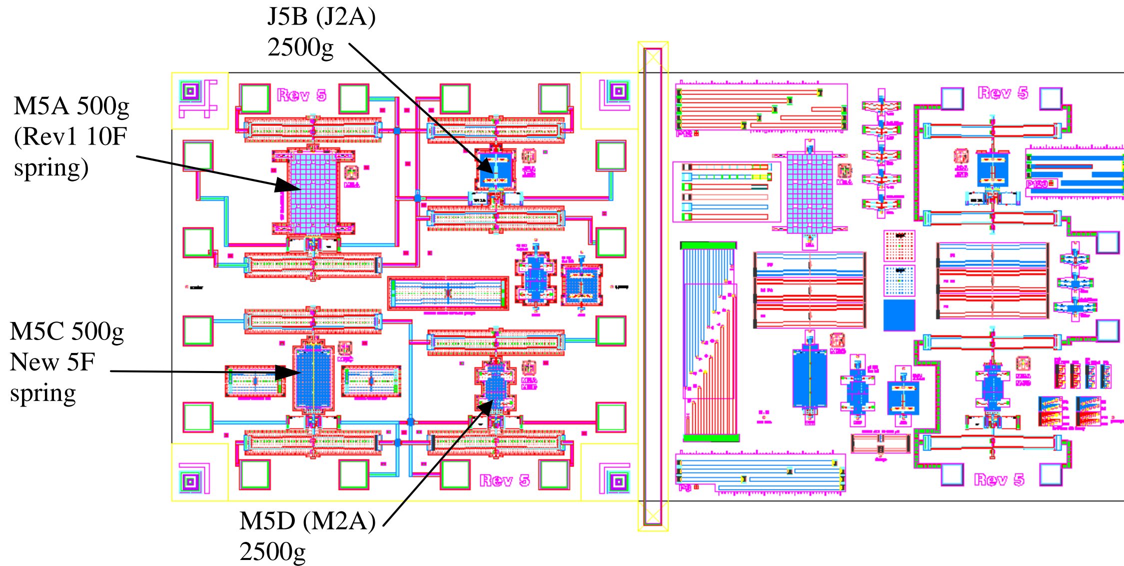

Figure 4. AutoCAD layout of Revision 5.

The main purpose of Revision 5 was to include devices with no dimples and also to fabricate devices without the Poly 4 shadow mask so that an interferometer could measure the mass structure flatness. At the end of FY07, when Revision 5 was submitted, it was still not known whether the J-series devices would work, so 3 of the 4 devices on Revision 5 used the M-series design for the spring/mass topology. Half the module was devoted to test structures to evaluate the flatness of the mass structures and measure the force-displacement of the devices via interfacial force microscopy (IFM), a technique which is currently being developed for measurement of both in-plane and out-of-plane forces in the µN range. Additional information on Revision 5 can be found in Appendix A, Section A.2.

1.1.7 Revision 6

The layout for Revision 6 is shown in Figure 5.

Reticle Set: RS686
Date Submitted: 3/31/08 (Checkplots arrive)
Date Completed: Expected 5/28/08 (out of fab)

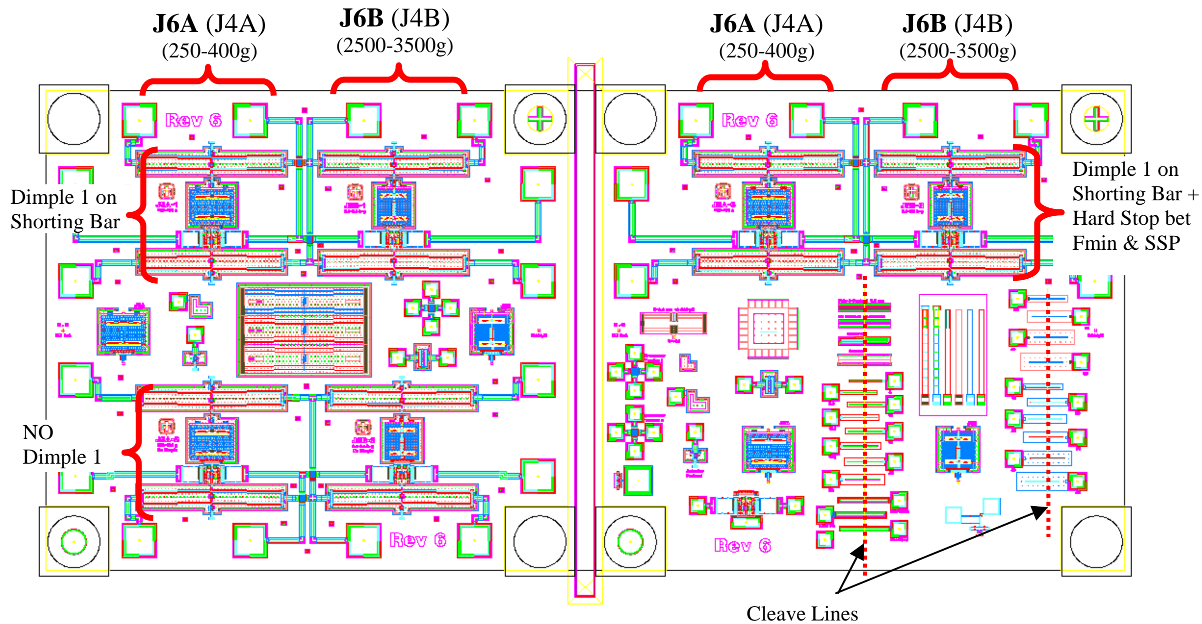

Figure 5. AutoCAD layout for Revision 6.

The main purpose of Revision 6 was to demonstrate top-down sputtering metallization of contact sidewalls while preventing shorting of the actuators, mechanisms, and traces. Mike Baker had success in the past with creating a special shadow mask for the bi-stable relays, so confidence was high that this approach would work for the shock switch. No new bi-stable mechanisms were designed for this revision. All bi-stable mechanism on Revision 6 came from Revision 4 so that J6A is the same as J4A, and J6B is the same as J4B with the exception that dimples around the edges of all devices on Revision 6 were removed.

Toward the end of FY07, a lean six-sigma event was conducted to look at ways of reducing the number of particles generated during the evaporative metallization process (different from the top-down sputter process). Handling steps (tweezering) and clamping the die in the fixture were identified as the main causes for particle generation. The FY07 report [Mitchell et al. 2008] includes a checklist in the appendix that details the process developed to minimize particle generation during handling. Failure analysis [Mitchell et al. 2008, Walraven et al. 2008] illustrates shorting failures due to particles. The hope for Revision 6 was to bypass nearly all particle problems by using top-down sputtering.

The main advantage of the sputtering method is that the die does not need to be held upside down with a fixture. Instead, the die can be placed face-up on a plate, without any special fixture. This should result in fewer particulate shorts due to less handling and no need for clamping the die in a fixture. The main risk is that sputtering is not line-of-site as is evaporative deposition, and it may be more difficult to design the shadow mask. A number of structures were included on Revision 6 to test different features and elements of the design for shorts. Some structures were electrical, and others were designed for cleaving to examine cross-sections under a microscope. By testing these structures, and performing self-tests of the devices, the top-down sputter approach was determined to be successful prior to the Revision 7 submission.

Two devices were included on Revision 6 to test whether preloading the mechanism could reduce sensitivity to frequency content during a shock event. Variations of J6A and J6B were included with and without Dimple 1 under the shorting bar because it was not known whether top-down sputtering would result in a welding failure mode. Table 1, containing the model results for Revision 4 is also applicable to Revision 6.

1.1.8 Revision 7

The layout for Revision 7 is shown in Figure 6.

Reticle Set: RS720
Date Submitted: July 30, 2008

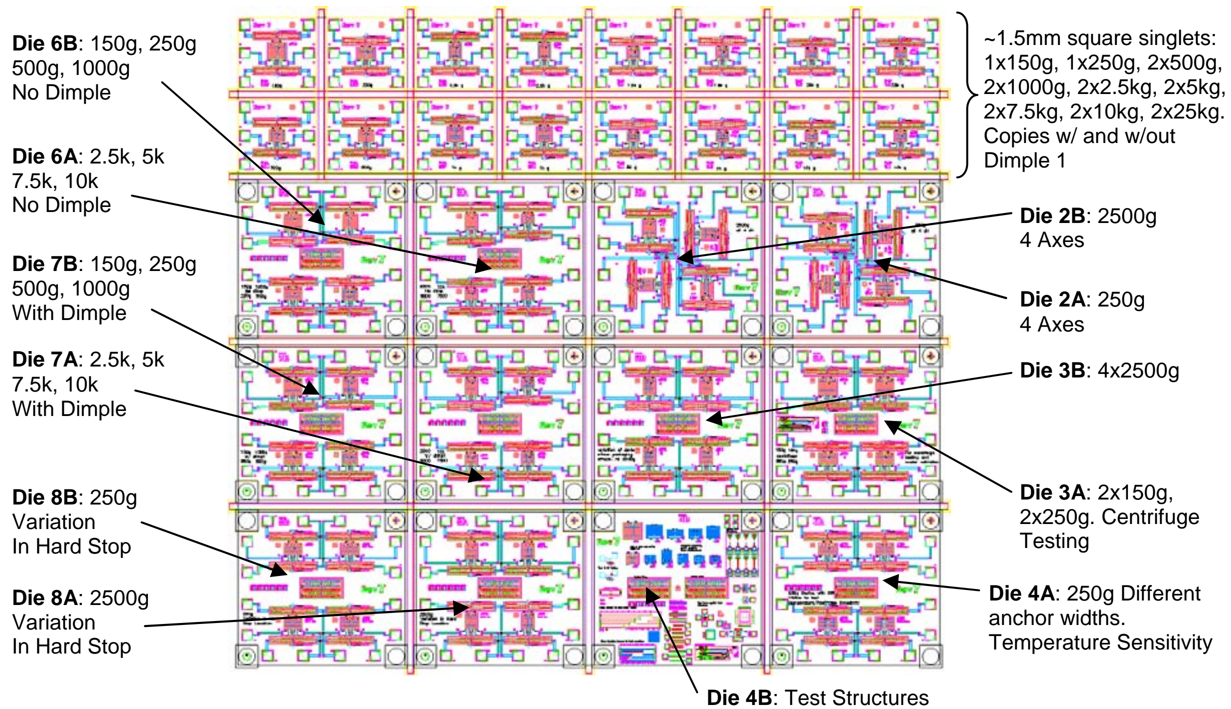

Figure 6. AutoCAD layout for Revision 7.
Note: In Figure 6, above, the devices have no dimples unless otherwise stated.

The Revision 7 design submission served many different purposes. The main reason for running an entire reticle set was to test nitride isolation between the thermal actuators, mechanism, and contacts. Although floating the contacts provides a solution for eliminating the so-called welding failure mode, nitride isolation would allow a future reduction in the number of wires and simplify implementation details for the surrounding customer system. If, for some reason, the nitride isolation steps result in new failure modes, fabrication process steps associated with nitride isolation can be skipped, thereby producing wafers without nitride isolation. To handle this later case (skip nitride isolation) electrical traces on the die were implemented to also float the contacts. Test structures specifically for the nitride isolation were included on Die 4B. Die labeling is based on traditional labeling of SUMMiT V lots and dicing maps, where the reticle is rotated 90 degrees counter clockwise.

One major design variation in Revision 7 was the use of a smaller die size, about 1.5mm×1.5mm, containing a single shock sensor. This allows for a smaller package with fewer pins or wires. Another change was the standardization of the mass structures used for J-series devices. The array of spring designs and the ease with which the mass can be modified allows for a large range of acceleration thresholds from 150g to 24,000g. Still another modification in Revision 7 was the reduction of the anchor width to further reduce sensitivity to residual stress and temperature (see [Mitchell et al. 2008] for some detail).

A full die of test structures was included in Revision 7, and many die were designed for specific experiments, such as temperature sensitivity and hard stop locations for mitigating the effects of frequency content. All the devices were re-optimized using a higher fidelity model (finer mesh) than formerly implemented. One die contains 2 copies of the 150g and 250g devices, along with test structures for measuring line width and residual stress. At these lower g-levels a centrifuge can be used to measure quasi-static set points of the devices enabling model validation.

Table 2 gives a summary of model results, including threshold acceleration uncertainties. Note that the model used for these calculations (quasi-static 2d shell element model described in chapter 2) is the same model as used for Revision 4 (see Table 1). Individual devices listed in column one of Table 2 can be mapped to specific die shown Figure 6 by using the g's column in Table 2. For example, all 150g devices in Figure 6 are J7A.

Table 2. Summary of Model Results for Revision 7

					Results from Monte Carlo Simulation		
		Mass	*MidWidth*	Middle	**Mean Force**	**Accel**	**Uncertainty**
Device	**Spring**	mg	um	Rows	uN	g's	Q(0.025,0.975)
J7A	1F	7.262E-04	124	3+12	-1.045	147	[126, 156]
J7B	1F	4.122E-04	36	3+1	-1.053	260	[227, 277]
J7C	2F	3.874E-04	44	3+2	-1.968	518	[454, 551]
J7D	5F	4.851E-04	108	2+11	-4.900	1030	[930, 1084]
J7E	10F	4.624E-04	132	2+14	-11.005	2426	[2159, 2549]
J7F	10F	2.251E-04	28	2+1	-10.940	4955	[4401, 5209]
J7G	20F	2.755E-04	52	2+4	-21.072	7796	[7053, 8177]
J7H	20F	2.040E-04	20	2+0	-20.332	10160	[9136, 10707]
J7K	50F	2.116E-04	20	2+0	-50.372	24265	[22933, 24993]

1.2 Fault Tree Analysis

In the beginning of FY08 (October '07), a fault tree analysis was started to better understand design issues and failure modes. This work led to the development of some of the test structures used on Revision 5, 6, and 7. It is recommended that the fault tree continue to be updated, and that a failure mode and effects analysis (FMEA) be completed, as a means of documenting what efforts are made to work around or mitigate various failure modes. It is advantageous to use the fault tree and FMEA as a tool during the design of future devices, to increase the probability of success.

1.3 Test Structures

In all design submissions, a number of test structures were included, either on the same die as the shock sensors, or on a separate die, or both. The most consistently used test structures are the residual stress, or bowtie, structures. These structures are explained in detail in the FY07 report [Mitchell et al. 2008]. Descriptions of some of the other structures are included in Appendix A of the present report.

2. Modeling

The FY07 report [Mitchell et al. 2008] provides a detailed description of the modeling effort for the shock switch. The emphasis in this report is modeling of the J-series design. There are 4 main models used to design the J-series device.

The first-stage model is the simplified beam-element quarter-model that is identical to the one used to design the M-series devices. This model does not take into account the compliance of the frame, which is significant to the performance of the J-series.

The second-stage model is a beam-element model that includes the frame. However, the use of a beam element for the frame assumes a solid mass which is inaccurate. This model runs efficiently enough to be used for optimization.

The third-stage model is a 2D shell-element model that includes the etch holes in the frame. The beam element and 2D shell element models are all parametric, built using a similar set of design parameters, as shown in Figure 7.

The fourth-stage is a full 3D model, generated from the MEMS design tools in AutoCAD. Prior to creating the 3D model, the design in AutoCAD is modified to take into account the 0.1µm edge bias. The 3D model has been used for modal analysis of Revision 4 designs, as well as to study the effect of residual stress on the curvature of the mass. The problems with the 3D models are (1) they are not parametric, (2) they take a very long time to solve, and (3) they often have convergence problems.

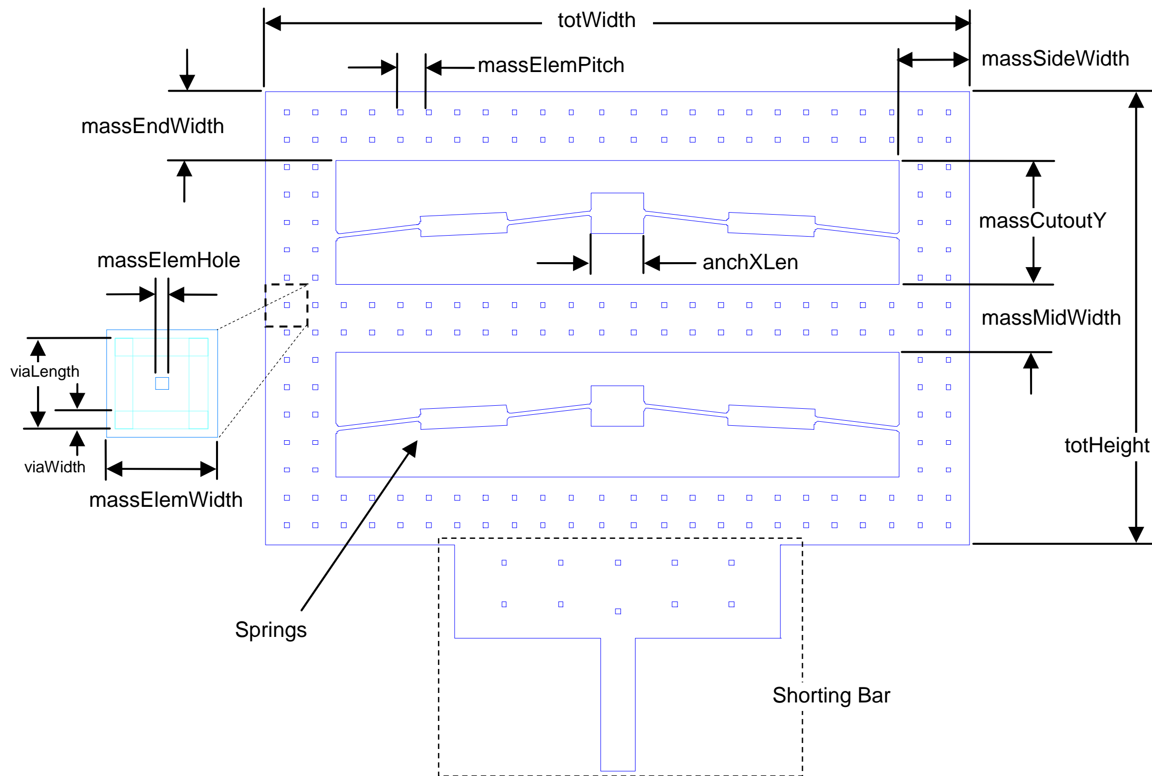

Figure 7. Design parameters used in J-series models; note this particular device has 2 mass rows.

Figure 7 shows the design parameters used to describe the geometry of the frame in the J-series models. The springs still use the same parameterization used in the original bi-stable mechanism literature [Mitchell et al. 2006, Wittwer et al. 2008, Mitchell et al. 2008, Wittwer et al., 2006]. For a given spring design, Figure 7 above shows the minimum mass, where *massMidWidth* is the same as *massEndWidth*. Additional mass can be added by including additional rows of mass elements in the middle to add to *massMidWidth*. This method of adding mass is beneficial because it keeps the additional mass closer to the center of gravity. Adding the mass to the outer edges will lower the frequency of some of the rocking vibrational modes, and that may not be desirable. The design of the shorting bar is based on the need for ensuring that sufficient polysilicon is exposed (from under that shadow mask) to get the metal on the sidewalls during metallization.

Because the size of the mass depends upon the spring design, each design has a different minimum mass. The width of the frame is based on the number of mass elements, and can be related using the following equation:

$massEndWidth = massElemWidth + (n-1) * massElemPitch$

where n is the number of mass elements (and therefore the number of holes).

A spreadsheet is used to calculate the mass based on the total width of the frame (*totWidth*) and the number of extra rows of mass elements that make up *massMidWidth*. Table 3 shows how

changing the masses for the different spring designs can give a large range of acceleration thresholds with just a few different spring designs.

Table 3 summarizes the force results, mass calculations, and the corresponding acceleration threshold in g's for different spring designs and masses. The gray shaded cells represent the mean force values from the finite element analysis (FEA)-based Monte Carlo Simulations described in the next section, but values for force in the right-most column are extrapolations. This table shows that with the given set of spring designs, it is possible to cover shock switch designs ranging from about 150g to 24,000g, although in some cases more than 15 rows of extra mass elements are required.

Table 3. Range of Set Points for Shock Switches Using Different Revision 7 Spring Designs

		# of Extra Rows in Middle of Mass			
Spring		**0**	**5**	**10**	**15**
1F	Force (μN)	-1.03964	-1.05439	-1.07312	-1.09185
	Mass (mg)	3.837E-04	5.264E-04	6.691E-04	8.118E-04
	g's	**276**	**204**	**163**	**137**
2F	Force (μN)	-1.88304	-1.97297	-2.03049	-2.08801
	Mass (mg)	3.389E-04	4.602E-04	5.816E-04	7.030E-04
	g's	**566**	**437**	**356**	**303**
5F	Force (μN)	-4.70364	-4.93844	-4.91738	-4.89632
	Mass (mg)	2.382E-04	3.504E-04	4.626E-04	5.748E-04
	g's	**2013**	**1437**	**1084**	**868**
10F	Force (μN)	-10.7378	-11.0544	-11.0782	-11.6876
	Mass (mg)	2.068E-04	2.981E-04	3.894E-04	4.806E-04
	g's	**5293**	**3780**	**2900**	**2479**
20F	Force (μN)	-20.3324	-21.0922	-21.0336	-20.975
	Mass (mg)	2.040E-04	2.934E-04	3.828E-04	4.722E-04
	g's	**10160**	**7328**	**5601**	**4528**
50F	Force (μN)	-50.3721	-52.5425	-52.4879	-52.4333
	Mass (mg)	2.116E-04	3.061E-04	4.006E-04	4.950E-04
	g's	**24265**	**17498**	**13357**	**10797**

2.1 Convergence Issues

The 2D shell-element model for the J-series devices often runs into problems converging. This most often occurs at the point in the displacement of the mechanism where we see a transition in the buckling of the legs. It is not known exactly why there are convergence problems, but the problems occur when (a) using the full model as opposed to the half model (b) the middle segment of the frame is not very wide and/or (c) the semi-rigid portion of the spring is not meshed fine enough. Adding a slight offset to the load can help the full model converge, but that does not always work.

When looking at the effects of mesh refinement in the 2D model, it was first thought that the mesh of the frame needed to be refined, but it was in fact the mesh of the semi-rigid segment in the spring (the wider middle section) that required a finer mesh. The area where the springs

connect to the frame needs to be refined as well. Also, the size of the etch holes in the mass can have a significant effect on the force-displacement curve.

2.2 Bi-stable Mechanism Design Parameters

Throughout the different design revisions, pre-existing spring designs were used in the bi-stable mechanisms or they were re-optimized for new set points. More information about the optimization is included in the following section. Figure 8 below shows the parameterization for the springs in the bi-stable mechanism.

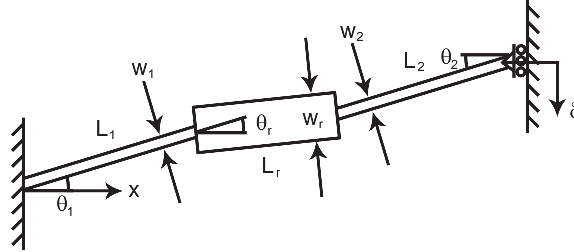

Figure 8. Design parameters for the bi-stable mechanisms.

Table 4 provides a summary of the bi-stable mechanism spring parameters for Revision 7, as well as the other design revisions. Note that a simplified notation has been used to show equality of subscripted parameters, i.e., $L_{1,2} = L_1 = L_2$. For clarity, a naming convention that uses both the revision number and the series type (M or J) was used in the table. For example, device M5D refers to a Revision 5 M-series device with D identifying a particular device on that die.

Table 4 can help compare the different spring designs from one design revision to the next. Spring designs were re-used wherever possible, but as explained in the following section, all the Revision 7 designs were re-optimized. For Revision 7, the 10F spring was based on the J4B design and the 5F spring was based on the J4C design. The J4B spring was nominally around -13 µN, so the Rev7 10F spring was modified slightly to bring the force closer to -10 µN. The J4C frame used a different mass structure, so the Revision 7 5F spring geometry was modified slightly to re-optimize it with the new mass. The 20F design is a new design selected from a set of optimization runs using a subset of starting points described in the FY07 report [Mitchell et al. 2008]. The 2F design is based on the J4A design, but re-optimized because of the new mass structure. The 1F design is based on the 2F design, re-optimized for an even lower force. The 50F spring is a completely new design.

Table 4. Summary of Spring Parameters for Different Designs

	Device	Spring	$L_{1,2}$ (μm)	$\theta_{1,2}$ (deg)	$w_{1,2}$ (μm)	L_r (μm)	θ_r (deg)	Mass (mg)
Rev 7								
	J7A	1F New	26	8.5	1.02	65	1.525	7.262E-04
	J7B	"	"	"	"	"	"	4.122E-04
	J7C	2F New	25	7.77	1.04	45	1.725	3.874E-04
	J7D	5F New	31.8	7.022	1.3	30	1.904	4.851E-04
	J7E	10F New	24	6.8	1.22	24	2.4	4.624E-04
	J7F	"	"	"	"	"	"	2.251E-04
	J7G	20F New	25	5.75	1.3	20	2.9	2.755E-04
	J7H	"	"	"	"	"	"	2.040E-04
	J7K	50F New	23.8	3.95	1.4	27.5	3.8	2.116E-04
Rev 6								
	J6A	[J4A]	26	7.77	1	45	1.725	[J4A]
	J6B	[J4B]	23.712	6.83	1.295	24.489	2.49	[J4B]
Rev 5								
	M5A	[Rev1-10F]	32.06	8.29	1.49	23.16	2.06	
	M5C	New	20.5	7.773	1.09	28.7	2.127	9.901E-04
	M5D	[M2A]	22.53	6.99	1.16	23.34	2.37	[M2A]
	J5B	[J2A]	23.712	6.83	1.295	24.489	2.49	[J2A]
Rev 4								
	J4A	[J3A]	26	7.77	1	45	1.725	4.570E-04
	J4C	[J3C]	31.8	7.022	1.3	30	1.904	6.130E-04
	J4B	[J2A]	23.712	6.83	1.295	24.489	2.49	4.100E-04
	J4D	[J2B]	"	"	"	"	"	1.970E-04
Rev 3								
	J3A & J3B	New	26	7.77	1	45	1.725	
	J3C & J3D	New	31.8	7.022	1.3	30	1.904	
	J3E	[Mod J2A]	23.712	6.83	1.2	24.489	2.49	
	J3F	New	19	4.892	1	15	3.262	
	M3A,B,&C	[M2A]	22.53	6.99	1.16	23.34	2.37	
	M3D	[M2D]	23.68	3.754	1.21	15.05	4.373	
Rev 2								
	M2A	New	22.53	6.99	1.16	23.34	2.37	4.053E-04
	M2B	"	"	"	"	"	"	2.022E-04
	M2C	"	"	"	"	"	"	1.037E-04
	M2D	New	23.68	3.754	1.21	15.05	4.373	1.985E-04
	J2A	New	23.712	6.83	1.295	24.489	2.49	4.302E-04
	J2B	"	"	"	"	"	"	2.105E-04
	J2C	New	15.675	4.892	1	15	3.262	2.224E-04
	J2D	New	23.8	3.95	1.36	15.02	4.65	2.299E-04
Rev 1								
		Rev1-2F	30.86	6.84	1	15.89	0.726	
		Rev1-5F	24.74	9.57	1.1	17.71	1.87	
		Rev1-10F	32.06	8.29	1.49	23.16	2.06	
		Rev1-20F	29.19	5.61	1.41	16.77	2.44	

2.3 Optimization of the Bi-stable Mechanisms

The FY07 report [Mitchell et al. 2008] provides background on how springs are designed to be insensitive to edge bias variations resulting from imperfect fabrication. The importance of this was made evident from shock test results from the J4D device. Originally designed to be a 5,000g device, it was actually switching at around 2500g. After modeling the device with an

updated model and finer mesh, it was discovered that the device was suboptimal with respect to edge bias variation. It was far more sensitive to edge bias than the original model indicated.

Figure 9 shows a graph of F_{min} vs. edge bias for the J4D device using the updated model. If the edge bias is less than the nominal 0.1 µm, F_{min} is significantly lower in magnitude. In-fab measurements of critical-dimension features on a couple of wafers from the RS661 lot showed a mean of 0.045 µm for the Poly2 edge bias (ranging from 0.029 to 0.062 µm) and a mean of 0.127 µm for the Poly3 edge bias (ranging from 0.107 to 0.145 µm). This provides significant evidence that the lower than expected threshold (2500g versus 5000g) measured for the J4D could be due to edge bias variation.

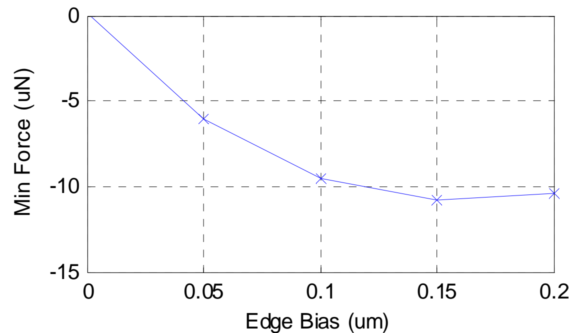

Figure 9. Model results showing Fmin vs. edge bias for the J4D design.

The Revision 7 devices were all optimized using the updated models. For the Revision 7 devices, the mass structure was made the same as that used in test structures on the Revision 5 die and the J4B device. Previous spring designs were used as a starting point the different spring designs, but in most cases devices had to be re-optimized or fine-tuned because the mass structure affected the force-displacement curve.

The Revision 7 devices were first optimized using the SCBM beam-element model (*ansys_scbm_beam4.mac*). SCBM stands for Stress-Compensated Bi-stable Mechanism – the official name for the J-series topology shown in Figure 7. The MATLAB script, *script_SCBM_edgebias.m*, is used to determine sensitivity to edge bias, and the input parameters for each spring design are stored in separate m-files like the one shown in Appendix B.

After optimizing using the beam-element model, the devices must be re-optimized (fine-tuned) using the 2D shell-element model (*ansys_scbm_2Dshell_half.mac*) because the beam-element model only approximates frame effects. Note that this assumes the 2D model is more accurate than the beam-element model (the comparison to Revision 4 data suggests that it is). Usually, the geometry parameters only need fine tuning and the optimization can be done manually. The ANSYS model is run using a batch script (*run_ansys_edgebias.bat*) that runs the 2D model for 5 different values of edge bias. A MATLAB script (*analyze_edgebias_uncertainty.m*) is used to create a F_{min} vs. Edge Bias curve that is fit using regression (the red curves in Figure 11 below), and a Monte Carlo simulation is used to determine the mean value for F_{min} assuming a uniform distribution of edge bias with the range [-0.18µm,-0.02µm] and a nominal edge bias of -0.10 µm. Figure 10 below shows an example of the Monte Carlo Simulation results, plotted as a histogram. It is important to realize that the predicted distribution is non-normal, and therefore the nominal value for F_{min} is not the same as the expected mean value. Instead of describing the

95% uncertainty region for F_{min} as a mean ±2 standard deviations (the blue and red lines, respectively), the 95% interval defined as the 0.025 and 0.975 quantiles (the green dashed lines) is reported. These are the values reported in Table 1 and Table 2.

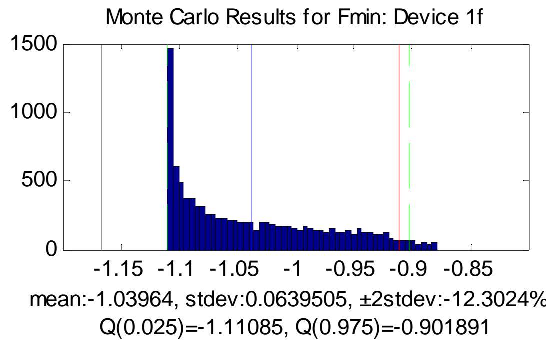

Figure 10. Example of the Monte Carlo Simulation results for the Revision 7 1F design.

In the J-series design, the force is slightly dependent on the width of the middle segment of the frame (*massMidWidth*). To address this in Revision 7, each spring design was evaluated for the minimum mass (0 additional rows), as well as for the +5 rows and +10 rows cases. Figure 11 below shows the F_{min} vs. Edge Bias curve for the Revision 7 2F spring design with 0, +5, and +10 extra rows (*massMidWidth*=28µm, 68µm, and 108µm, respectively). Note that the value of edge bias associated with the minimum force is independent of the number of mass rows and thus the device remains robust to edge bias variations even when the mass changes. This then allows one to use Table 3 to design devices with a range of set points without re-optimizing the spring designs.

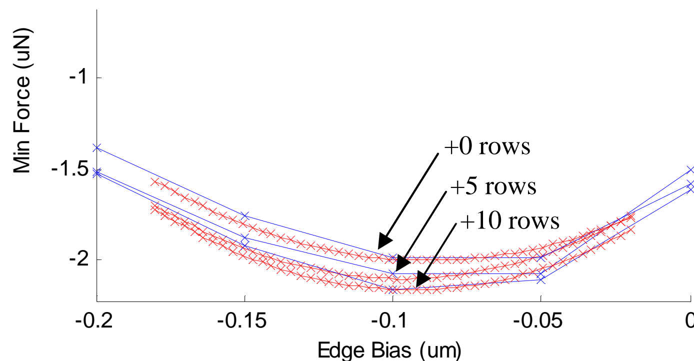

Figure 11. Curves showing sensitivity of Fmin to massMidWith.

2.4 Effect of Temperature on the Set Point

Testing in FY08 showed that shock switches (packaged in the FY08 test package [Baker et al. 2008]) sometimes self-closed when subjected to very cold temperatures. This was surprising given that the model for the J-series design predicts devices to be fairly insensitive to residual stresses. If the substrate is constrained to *not* displace as a result of temperature (see Figure 12 below), then a range of -70°C to 140°C results in a very small change in set point which is not enough to cause the mechanism to self-close.

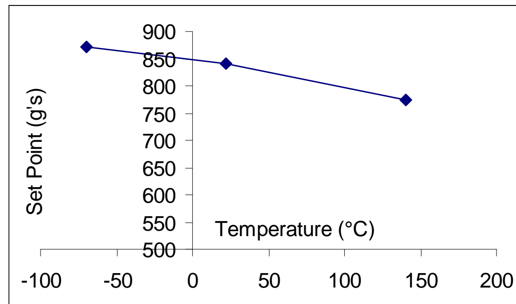

Figure 12. Effect of temperature on the set point (J4C), assuming a rigid substrate.

The coefficients of thermal expansion for JM7000 (used in die attach), LCC, and aluminum housing are all higher than for silicon, so when the device cools the silicon will not shrink as much as the package. This would cause a residual stress that could result in the anchor points moving more than the normal expansion/contraction of the silicon. In this case, getting colder might cause the device to self-close, while getting hotter should result in a higher set point. So far, tests have shown that no devices self-close for the following cases: (1) bare die (2) metalized die or (3) die attached to LCC. The next step is to package these same devices in the FY08 test packages and perform the same thermal test.

2.5 Positioning the Hard Stop to Reduce Vibration Sensitivity

One idea for mitigating sensitivity to vibration is to place the hard stop at or near the second stable position. There are a variety of positions that may be studied. At one extreme, the hard stop is positioned similar to that indicated in Figure 13. Note that the schematic shows the hard stop and the fabricated position and second stable position shown as dotted lines. The hard stop location is indicated on the force vs. displacement plot in Figure 14. In this case, the mass would be resting against the hard stop when in the open position; this may be undesirable as noted below. The other extreme is where the hard stop is located far away (and to the right on the force versus displacement curve) from the second stable position and beyond where it is expected to move under most circumstances; this is how most revisions were implemented. At the time of this writing, evidence is not yet in on whether moving the hard stop closer to the 2nd stable position will suppress vibration in the open condition and thereby reduce frequency response at frequencies between 1 kHz to 20 kHz. The hope is that moving the hard stop closer will cause the device to impact the hard stop rather than building up a large resonant amplitude. The idea being that impacts act as a damping mechanism. The coefficient of restitution for polysilicon-on-polysilicon is assumed to be 0.5.

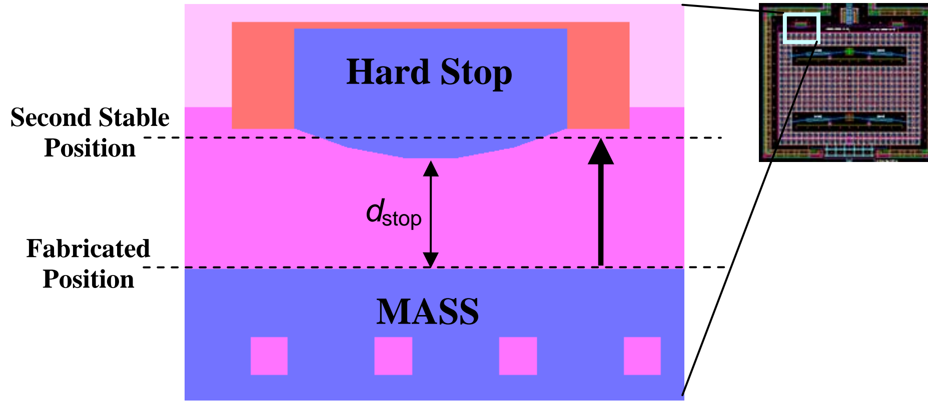

Figure 13. Schematic showing the hard stop position relative to the mass.

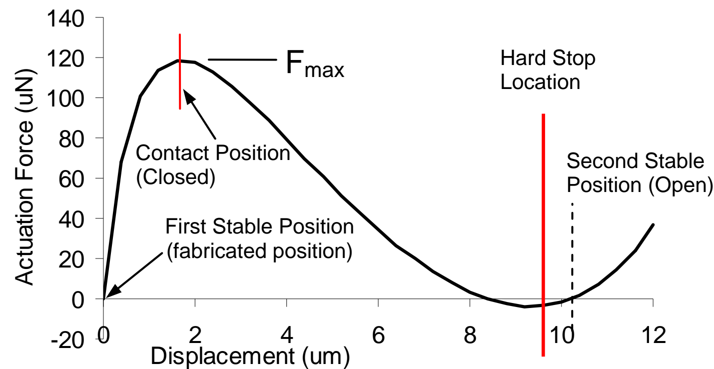

Figure 14. Force vs. displacement showing hard stop location.

If successful, the benefit of this approach would be less sensitivity to vibration, ringing and high frequency content, without requiring a special packaging solution. The potential problems with this approach are:

1. The uncertainty in the location of the SSP might result in contact at rest, which could lead to long-term reliability problems, potentially welding/sticking the device to a hard stop
2. Particle generation due to the impacting surfaces
3. The device might stick to the hard stop, causing an increase in the threshold acceleration
4. The design of the spacing for the actuator, contact, and hard stop is much more difficult, and tolerances must be taken into account.

Moving the hard stops closer increases the difficulty of designing the appropriate gaps between the actuators, mechanism, and latching contacts. This requires a detailed tolerance analysis to prevent 3 possible failure modes:

1. Failure of the actuator to latch the contacts
2. Failure of the actuator to toggle the mechanism to the second stable position (SSP)
3. Movement of the latched contacts required when toggling the mechanism

The design of the gaps is detailed in the FY07 report [Mitchell et al. 2008]. Summary tables of the gaps for Revision 4 and Revision 7 designs are included in Appendix A. Figure 15 shows schematics and the dimensions listed in the tables.

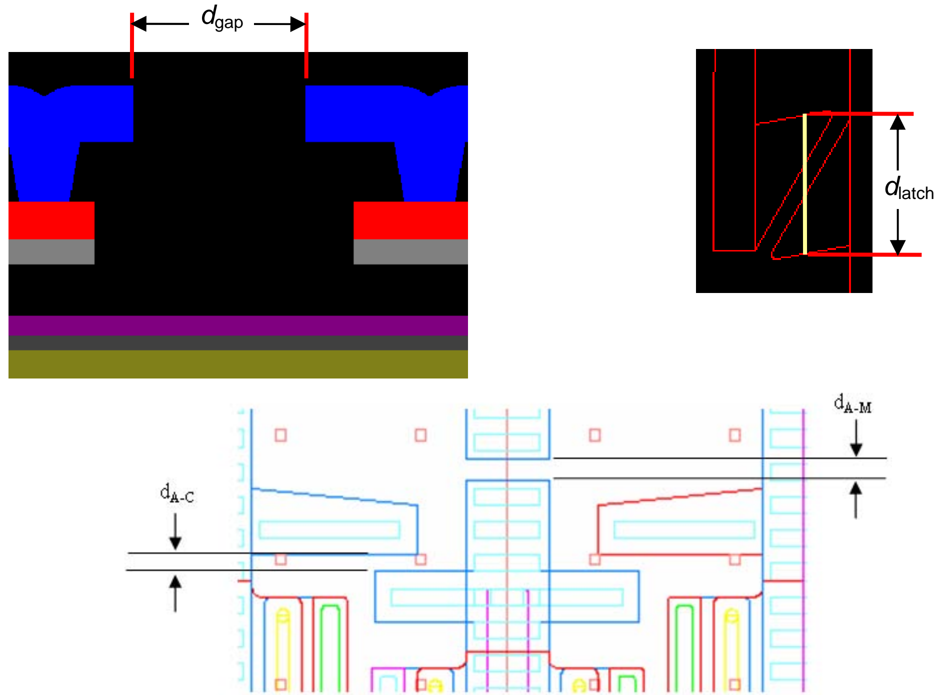

Figure 15. Schematics showing the as-drawn contact gap (dgap), latch distance (dlatch), actuator-to-contact spacing (dA-C), and actuator-to-mechanism spacing (dA-M).

2.6 Dynamic Simulations

A detailed description of the dynamic model is provided in the FY07 report [Mitchell et al. 2008]. One feature added to the model this year was the introduction of a new input function, known as a WAVSYN pulse. Figure 16 shows an example time history of a WAVSYN pulse function. This function was used in testing to circumvent the limited amplitudes achievable with the shaker when using traditional sine wave inputs [Epp et al. 2008]. A detailed description of the test is provided in [Epp et al. 2008], and Figure 17 shows an example of the model results for device J4A with different quality factors. A lower quality factor (i.e., higher damping) would be preferable.

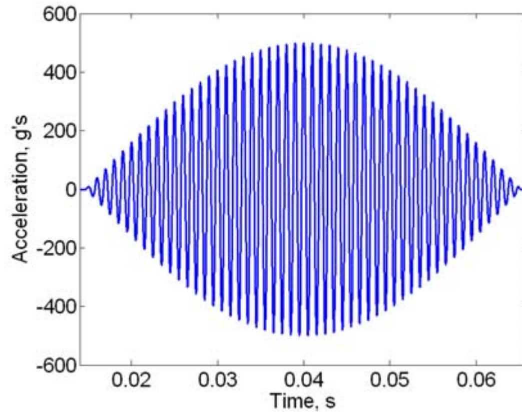

Figure 16. 500 g's 1000 Hz WAVSYN pulse with 101 half sines [Epp et al. 2008].

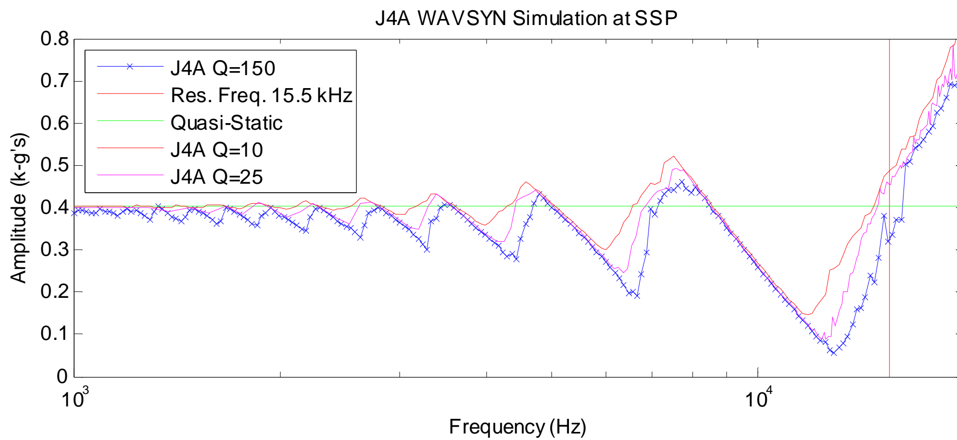

Figure 17. Model results for device J4A in response to WAVSYN inputs, showing the amplitude at which the switch closes.

Figure 18 through Figure 21 show the displacement acceleration amplitude vs. frequency plots for dynamic simulations of the J7B device using a WAVSYN input. For all 4 simulations, the quality factor was Q=150 and the coefficient of restitution was set to 0.5.

These plots provide theoretical evidence that the hard stop can be used to reduce the sensitivity to vibration, particularly if the device is preloaded (Figure 21) or the hard stop is placed very close to the second stable position (Figure 20).

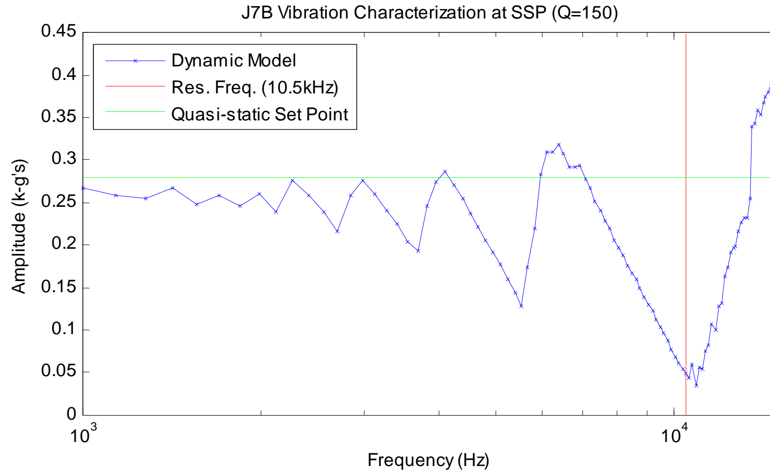

Figure 18. Hard stop at 12 µm (the nominal design).

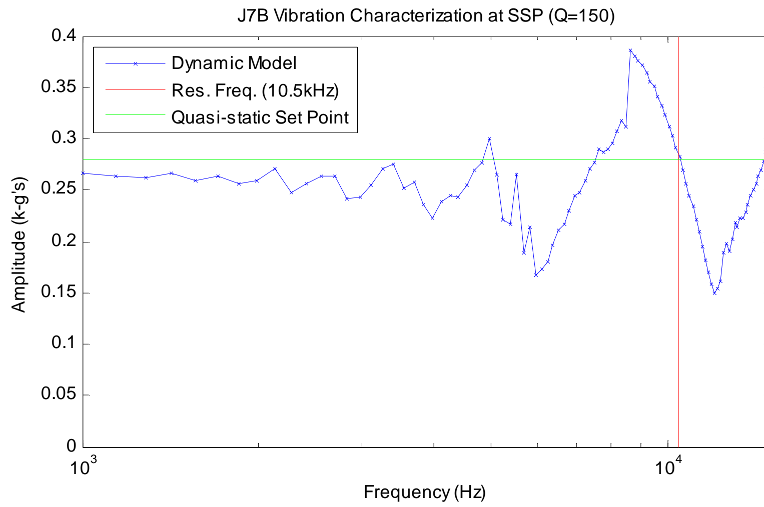

Figure 19. Hard stop at 10.9 µm, conservative distance from SSP.

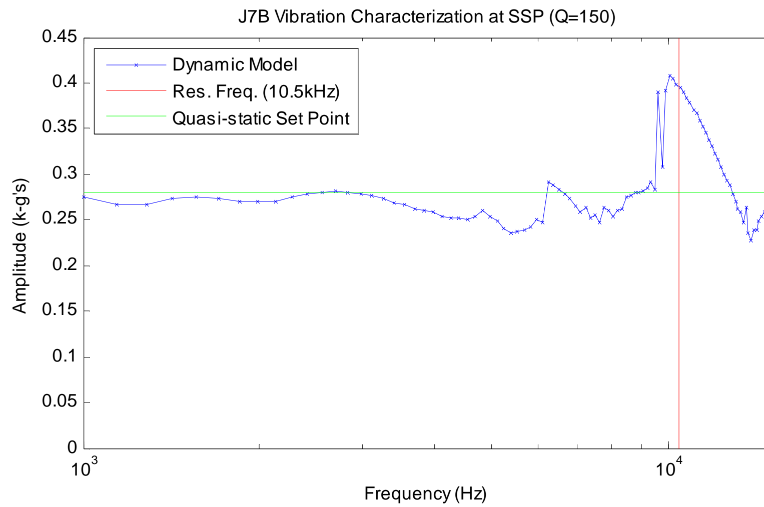

Figure 20. Hard stop at 10.6 µm, almost touching at SSP.

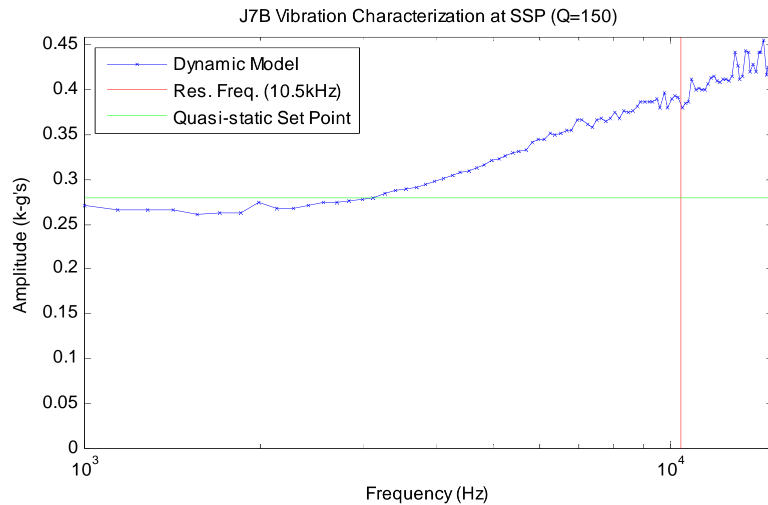

Figure 21. Hard stop at 10.0 μm, preloaded against the hard stop.

2.7 Model Validation

For a detailed discussion of the testing and model validation efforts in FY08, see the companion report, "The Sandia MEMS Passive Shock Sensor: FY08 Testing for Functionality, Model Validation, and Technology Readiness" [Epp et al. 2008]. The two tables in this section represent only a small selection of the results in that report. Most of the testing in FY08 was done on Revision 4 parts, where all devices were the J-series design. Table 5 shows a comparison between the shock test results and modeled acceleration thresholds. Table 6 compares the measured and modeled resonant frequencies. In both cases, the model results agree quite well with the measured results, except for J4D as discussed in Section 2.3.

Table 5. Comparison of Measured and Modeled Results for Revision 4 Shock Thresholds [Epp et al. 2008].

	Measured Threshold Bounds		Modeled Threshold Bounds 95% Confidence Level	
Switch	**Low (g's)**	**High (g's)**	**Low (g's)**	**High (g's)**
J4A-D	250	750	329	406
J4C-D	750	1500	688	843
J4B	2500	3000	2517	3327
J4D	2000	3000	1638	5342

Table 6. Comparison of Average Measured Resonant Frequencies to Modeled Results [Epp et al. 2008].

	Closed Position		Open Position	
Device	**Measured (kHz)**	**Modeled (kHz) ±0.02**	**Measured (kHz)**	**Modeled (kHz) ±0.02**
J4A-D	55 ± 4	49	16 ± 6	16
J4C-D	63 ± 3	74	21 ± 2	18
J4B	134 ± 6	125	43 ± 2	40
J4D	106 ± 7	167	46 ± 5	57

3. Conclusion

This report summarized the design and modeling activities for the MEMS passive shock sensor and is intended for use as a reference to compare the different designs. It provided a description of past design revisions, but focused on the development of Revisions 4-7. The procedure was given for analyzing the J-series designs with a new 2D shell-element model. The results of new dynamic simulations showed that positioning the hard stop close to the second stable position may help to reduce the effect of vibration on the threshold acceleration, but there may be disadvantages to this approach.

4. Future Work

It is expected that as the shock switch technology advances, modeling and analysis will continue to be needed in the design of new devices and to investigate possible causes for observations made during testing.

Model validation efforts should continue, particularly on effects of residual stress induced through packaging and temperature. Resonant frequency measurements and centrifuge measurements are currently the best for validating bi-stable mechanism models. When shock threshold are above centrifuge limits, drop-table testing is valuable for bracketing the response. If measured values of the acceleration thresholds are outside of the 95% uncertainty ranges given in Table 1 and Table 2, then additional modeling work may be required.

The dynamic model is based on a lumped mass and nonlinear force-displacement curve. While it can provide valuable insight into the behavior of the shock switch, it does not include off-axis acceleration effects, the influence of other vibration modes, or other non-idealities. Further development of the dynamic model will require additional testing and model validation.

5. References

Baker, M.S., C. Gustafson, M. Girardi, R.W. Schroeder, R.L. Hamm, B.D. Young, R.J. Brown, J.T. Slanina, F. Olivas, J.R. Dokos, R.C. Clemens, J.A. Mitchell, M.R. Brake, J.W. Wittwer, D.S. Epp, J.A. Walraven, *The Sandia MEMS Passive Shock Sensor: FY08 Packaging*, SAND2008-5967, Sandia National Laboratories, Albuquerque, NM, 2008.

Epp, D.S., J. Blecke, M.R. Brake, M.S. Baker, J.W. Wittwer, R.C. Clemens, J.A. Mitchell, J.A. Walraven, *The Sandia MEMS Passive Shock Sensor: FY08 Testing for Functionality, Model Validation, and Technology Readiness*, (submitted as a SAND report in 2008), Sandia National Laboratories, Albuquerque, NM, 2008.

Mitchell, J.A., M.S. Baker, J. Blecke, R.C. Clemens, D.A. Crowson, D.S. Epp, J.E. Houston, J.A. Walraven, J.W. Wittwer, *The Sandia MEMS Passive Shock Sensor: FY07 Maturation Activities*, SAND2008-5184, Sandia National Laboratories, Albuquerque, NM, 2008.

Mitchell, J.A., J.W. Wittwer, M.S. Baker, N. Spencer, K.R. Pohl, R.C. Clemens, D.S. Epp, J.C. Gilkey, L.M. Phinney, W. Wilbanks, W.Y. Lu, 2006, *On the Design, Packaging and Testing of Micro- and Meso-scale Inertial G-Relays*, SAND2006-5806, Sandia National Laboratories, Albuquerque, NM. 2006.

Walraven, J.A., M.S. Baker, J.W. Wittwer, D.S. Epp, M.R. Brake, R.C. Clemens, J.A. Mitchell, *The Sandia MEMS Passive Shock Sensor: FY08 Failure Analysis Activities*, SAND2008-5185. Sandia National Laboratories, Albuquerque, NM, 2008.

Wittwer, J.W., Baker, M.S. and Howell, L.H., Robust Design and Model Validation of Nonlinear Compliant Micromechanisms, in *Journal of Microelectromechanical Systems*, Transactions of the IEEE and ASME, vol. 15, No. 1, pp. 33-41, February 2006.

Wittwer, J.W., M.S. Baker, D.S. Epp, J.A. Mitchell, MEMS Passive Latching Mechanical Shock Sensor, in *Proceedings of the 2008 ASME International Design Engineering Technical Conferences*, DETC2008-49178, August 3-6, 2008. New York City, New York, 2008.

Appendix A:
Reference Information and Revision Notes for Revisions 4, 5, 6, and 7

Contents

A.1 Revision 4 Notes 41
- A.1.1 Nomenclature 41
- A.1.2 Model Results and Design Parameters 41

A.2 Revision 5 Notes 42
- A.2.1 General Features 42
- A.2.2 Shock Switch Designs 42
- A.2.3 Test Structures 43

A.3 Revision 6 Notes 48
- A.3.1 General Features of the Production Die 48
- A.3.2 Test Structures 48

A.4 Revision 7 Notes 50
- A.4.1 Model Results and Design Parameters 50
- A.4.2 General Features 51
- A.4.3 Die-Specific Information 52
- A.4.4 Test Structures 53

Appendix A: Reference Information and Revision Notes for Revisions 4, 5, 6, and 7

A.1 Revision 4 Notes

This section and the proceeding 3 sections contain additional information and details pertaining to design Revisions 4 – 7. Most of these notes were compiled prior to submitting the design.

A.1.1 Nomenclature

"set point" :: The force or the corresponding g-level required to toggle the device closed
"as-drawn" :: Refers to the dimensions of the device in the layout drawings
F_{min} :: Minimum force or "set point"
SSP :: Second Stable Position relative to "as-drawn" position
F_{max} :: Maximum force
$x(F_{max})$ :: The position of the maximum force relative to the "as-drawn" position
FSP :: The first stable position relative to the "as-drawn" position
UEP :: Unstable equilibrium position relative to the "as-drawn" position
S_{max} :: Maximum stress in the device between the FSP and SSP

A.1.2 Model Results and Design Parameters

Table A-1. Nominal Quasi-static Analysis Results Using the 2D-Shell Model with a Fine Mesh

Device	Set Point g's	Mass mg	S_{max} MPa	F_{max} μN	$x(F_{max})$ μm	F_{min} μN	$x(F_{min})$ μm	FSP μm	UEP μm	SSP μm
J4A-D	404.6	4.570E-04	568.5	28.09	1.86	-1.81	8.52	0.0029	7.38	9.56
J4C-D	842.0	6.130E-04	750.1	85.95	1.79	-5.06	9.18	0.0024	7.93	10.32
J4B	3322.5	4.100E-04	1022.6	153.10	1.49	-13.36	7.17	0.0025	6.00	8.20
J4D	4938.5	1.970E-04	1001.7	146.33	1.60	-9.54	7.16	0.0025	6.18	8.05

Table A-2. Gaps and Spacing for the Mechanism, Actuators, and Contacts (see Figure 13 and Figure 15).

Device	d_{gap} (um)	d_{latch} (um)	d_{A-M} (um)	d_{A-C} (um)	d_{stop} (um)	$x_{contact}$ (um)	x_{stop} (um)
J4A-D	10.4	12.405	4.3	3.0	11.8	1.9	12
J4C-D	10.5	12.405	4.5	3.0	11.8	1.8	12
J4B	6.8	8.408	2.5	2.0	9.5	1.508	9.7
J4D	6.8	8.408	2.5	2.0	9.5	1.508	9.7

Table A-3. In-plane Resonant Frequencies Using the SDOF Analytical Model and Force-Displacement Curves Generated from the 2Dshell Model.

	First Stable Pos.		Second Stable Pos.	
	Period	Freq	Period	Freq
Device	(μs) ±0.05	kHz	(μs) ±0.1	kHz
J4A-D	20.61	49	64.7	15.5
J4C-D	13.60	74	54.6	18.3
J4B	8.00	125	25.1	39.9
J4D	5.98	167	17.6	56.8

A.2 Revision 5 Notes

A.2.1 General Features

- **All mechanisms will be made with no dimples.**
  - This should reduce the occurrence of friction-related failure modes. It might increase the occurrence of the mechanism sticking to the substrate after metallization.
  - There is strong evidence suggesting that Revision 2 failures were due mass interaction with dimples (i.e., pictures + observed friction)
  - We have strong evidence that we can design large masses with very soft springs that don't end up touching the lid or substrate when we don't use dimples.
  - The occurrence of the mechanism sticking to the substrate after metallization in the Revision 1 parts was low. Also, Revision 2 designs are supposed to be stiffer out-of-plane.
- **All devices will use the Revision 2 Actuators.**
  - This should reduce the occurrence of actuator failure due to sticking after metallization.
  - We did not observe any stuck Revision 2 actuators, so the improvements appear to have been 100% successful.
  - We will keep the dimples on the actuators to make sure the actuator can't rotate enough to get stuck to the substrate and make sure the tabs don't extend too far from below the lid.
- **Floating the contacts.**
  - This is our best option for eliminating the *actuator-to-mechanism welding* failure mode.
  - We cannot use nitride for electrical isolation on this run.

A.2.2 Shock Switch Designs

- From Revision 1, M-Series, 500g, 10μN spring, No Dimples on Mechanism
  - Act as the control. It is the highest g-level that provided consistent data from 2006 testing
- From Revision 2, M-Series, 2500k-g, 10μN spring, No Dimples on Mechanism
  - Only difference between Revision 2 is removing the dimples

- Revision 2 vs. Revision 1:
  - Spring design optimized for improved z-stiffness
  - Change in mass layout reduces sensitivity to residual stress
  - Used the same model to design as Revision 1
  - More thorough analysis than Revision 1 designs (see FY07 report [Mitchell et al. 2008])
- From Revision 2, J-Series, 2500k-g, slightly modified spring from optimal z-sensitivity design, No Dimples on the Mechanism
  - Only difference between Revision 2 is removing the dimples
  - J-Series is new, so want the g-level close to M-Series for comparison
  - Less sensitive to residual stress, more difficult to design/analyze than M-Series
  - Possibly more sensitive to stress gradient
- New Design: M-Series, 500g, 5 μN spring, No Dimples on Mechanism
  - M-Series because we currently have more confidence that they work
  - 500g to compare with the Revision 1 control
  - Mass modified to be less sensitive to residual stress (like Revision 2)
  - 5 μN spring was optimized for z-stiffness, but not used in any Revision 2 designs

A.2.3 Test Structures

As explained in Section 1.1.6, an entire 3×3 mm module was set aside in Revision 5 for test structures. Figure A-1 shows the AutoCAD layout for this module. Listed below are short descriptions of some of the test structures.

- Resonant frequency measurements at FSP and SSP
  - All of the 4 devices can be toggled manually between FSP and SSP and laser Doppler velocimeter (LDV) can be used to measure vibration modes.
- Measurement of SSP
  - Verniers on ends of bistable mechanisms to measure SSP
- Bow-Tie residual stress testers (for Package-Induced stresses, also)
  - P2 and P3 and P2/P3 test devices placed along the center line of each set of switches – in the same orientation as the springs on the mass. The size of the test structures are much larger than the springs, so this will lead to stresses averaged over a larger portion of the die.
  - These structures are meant to be analyzed using pattern matching, rather than by eye.
- Fixed-Fixed beam residual stress testers
  - Basically the same as in the TCVs – meant for automated parametric test
  - P12 and P3
- Curvature of Cantilever beams
  - Similar layout as TCVs – meant for automated parametric test system
  - P12 and P3
  - Combined P123 using the mass element from the J-Series design
- WYKO “Mushroom” structures for measuring curvature of plates
  - All 200×200 μm square, anchored at the center
  - P2, P3, and P2+P3 using mass element from J-Series

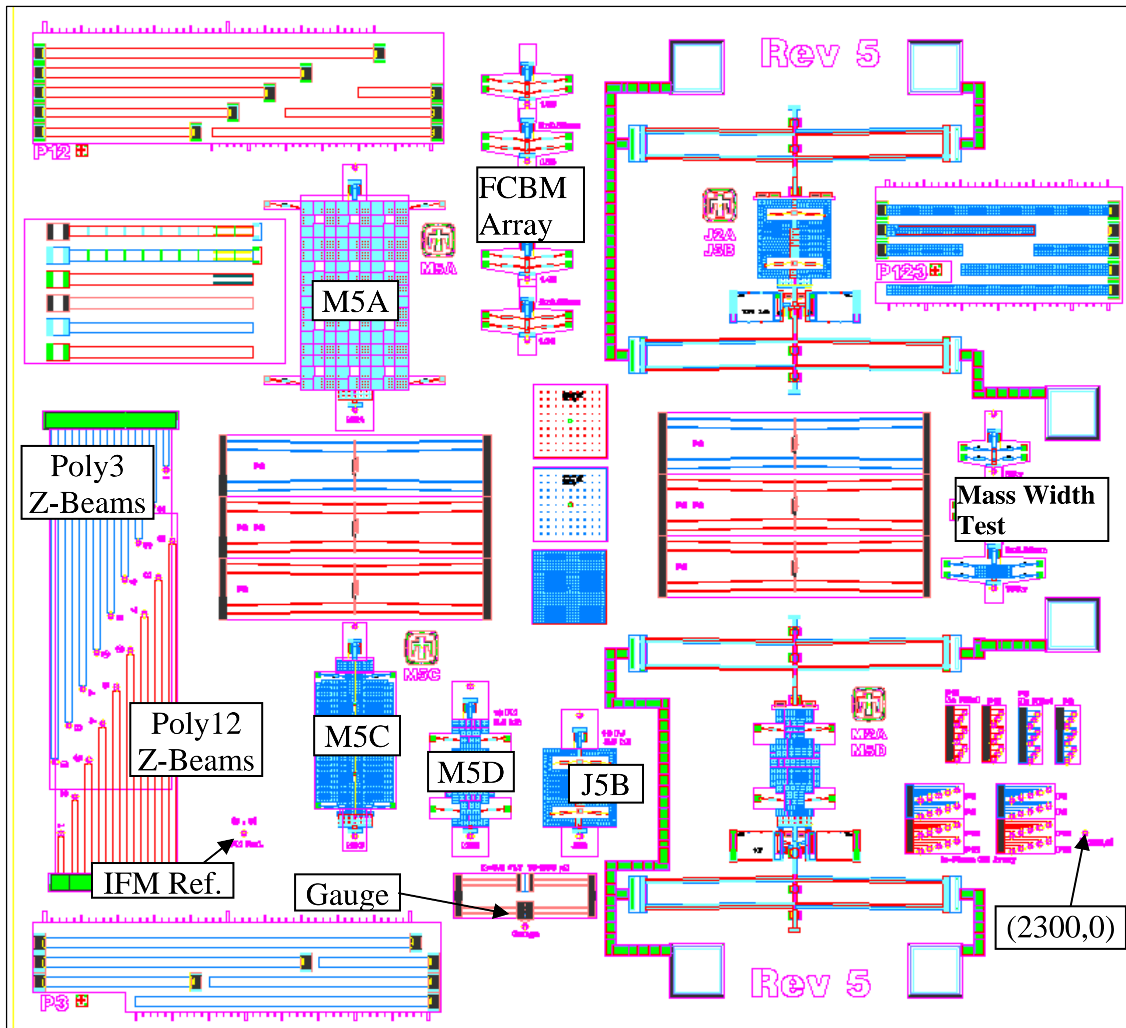

Figure A-1. Revision 5 test structure module.

The IFM Reference marks the origin from which the coordinates of other IFM marks are determined. X and Y locations listed below are relative to this origin. Another reference target is included at (2300,0) for verifying the orientation of the die (Figure A-2).

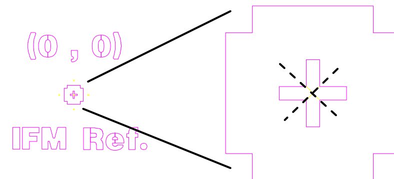

Figure A-2. IFM Target: position measured at center of Poly0 cross.

- IFM tests of all 4 designs
  - M5A and M5C in exact location, but M5B and M5D not (due to actuators)
  - Included an alignment feature for the IFM

- The table below provides the coordinates of the IFM targets for the as-fabricated position (FSP) and second stable position (SSP).

Target	X (µm)	Y (µm)
M5A (FSP)	304	1158.1
M5A (SSP)	304	1821.25
M5C (FSP)	304	-8.7
M5C (SSP)	304	565.95
M5D (FSP)	619	-8.7
M5D (SSP)	619	402.55
J5B (FSP)	919	-8.7
J5B (SSP)	919	322.55

- Force Gauge; IFM In-Plane force calibration verification
  - Force gauge with k=9.6±1.7 µN/µm (P3+P4)
  - Range: 10-230 µN
  - IFM Alignment target location listed below

Target	X (µm)	Y (µm)
Force Gauge	769	-254.862

- IFM or Nano-indenter to measure E, w, and t
  - See Figure A-3 for lab notes.
  - Cantilever beam array of different lengths (same as TCV design)
  - Width is 18 µm.
  - Center of target is 10 µm from the end of the beam (not counting edge bias)
  - Could also measure the natural frequency using LDV
  - Tables of alignment target locations are listed below

Target	X (µm)	Y (µm)
Poly12 Z beams, 1	-500	0
Poly12 Z beams, 2	-462	100
Poly12 Z beams, 3	-424	200
Poly12 Z beams, 4	-386	300
Poly12 Z beams, 5	-348	400
Poly12 Z beams, 6	-310	500
Poly12 Z beams, 7	-272	600
Poly12 Z beams, 8	-234	700
Poly12 Z beams, 9	-195	800

Target	X (µm)	Y (µm)
Poly3 Z beams, 1	-212	994.6
Poly3 Z beams, 2	-250	894.6
Poly3 Z beams, 3	-288	794.6
Poly3 Z beams, 4	-326	694.6
Poly3 Z beams, 5	-364	594.6
Poly3 Z beams, 6	-402	494.6
Poly3 Z beams, 7	-440	394.6
Poly3 Z beams, 8	-478	294.6
Poly3 Z beams, 9	-516	194.6

33 **PROJECT NAME** ______ **NOTEBOOK NO.** ______

Calibration of IFM & Determination of Thickness, Modulus, etc.

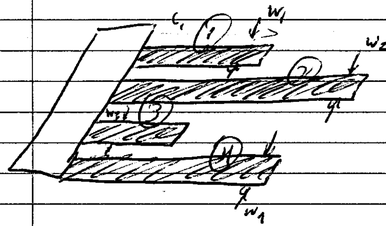

Cantilever Beams of 4 different Lengths

$$k = \frac{Ewt^3}{4L^3}$$

Assumptions:

(1) ΔL is negligible for each of the beams
(2) ΔE is identical for each of the beams
(3) Δt is identical " " " " "
(4) δ is known very precisely
(5) C is constant for the instrument
(6) Δw is identical for each beam

Instrument

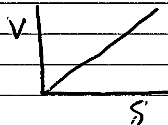

$F = VC$

$k = \frac{F}{\delta}$

$$\frac{V_1 C}{\delta_1} = k_1 = \frac{(E+\Delta E)(w_1+\Delta w)(t+\Delta t)^3}{4(L_1+\Delta L_1)^3} \quad \Delta L_1 \to 0 \quad \Delta V_1 \to 0 \quad \Delta\delta \to 0$$

$$\frac{V_2 C}{\delta_2} = k_2 = \frac{(E+\Delta E)(w_2+\Delta w)(t+\Delta t)^3}{4(L_2+\Delta L_2)} \quad \Delta L_2 \to 0 \quad \Delta V_2 \to 0 \quad \Delta\delta \to 0$$

$$\frac{V_3 C}{\delta_3} = k_3 = \frac{(E+\Delta E)(w_3+\Delta w)(t+\Delta t)^3}{4(L_3+\Delta L_3)} \quad \Delta L_3 \to 0 \quad \Delta V_3 \to 0 \quad \Delta\delta \to 0$$

$$\frac{V_4 C}{\delta_4} = k_4 = \frac{(E+\Delta E)(w_4+\Delta w)(t+\Delta t)^3}{4(L_4+\Delta L_4)} \quad \Delta L_4 \to 0 \quad \Delta V_4 \to 0 \quad \Delta\delta \to 0$$

Unknowns: $\begin{bmatrix} C \\ \Delta w \\ \Delta t \\ \Delta E \end{bmatrix}$

4 equations + 4 unknowns

How do you do the uncertainty analysis?
- Create a model in which you solve for ΔE, Δt, Δw, $\frac{1}{C}$ based on 4 measured k values
- Run MC Simulation in which you introduce uncertainty in δ, ΔL_1, ΔL_2, ΔL_3, ΔL_4, V_1, V_2, V_3, V_4, S_1, S_2, S_3, S_4, and deviations about ΔE, Δw, Δt

Design Variables: w_1, w_2, w_3, w_4
L_1, L_2, L_3, L_4

How does stress gradient and residual stress affect results? Probably not much

Could we use a nanoindenter for Parameters Testing?

What is the effect of the Support Compliance? Via Modeling will result in a fudge factor on the above equations. Slight effect.

SIGNATURE ______ **DATE** 10/4/07 **20**
READ AND UNDERSTOOD ______ **DATE** ______

Figure A-3. Lab book page: IFM or Nano-indenter to measure *E, w,* and *t*.

- IFM or WYKO measurements of Out-Of-Plane Motion
    - J5B and M5D designs with actuators to look at out-of-plane displacement as the devices are toggled
    - Not room to put actuators on the 500g designs

- IFM In-Plane cantilever beam array for measuring E, w, t,
    - See Figure A-3.
    - 4 copies of 5 different beam lengths
    - P2 and P3 beams, 1μm wide
    - Added bumpers to help align the IFM tip to get an accurate L.
    - Added fillets of 0.64 to account for local elasticity at the support

- Effect of Mass Size on Bi-stable Mechanisms (M5C spring design)
    - 3 different mass widths to check sensitivity to residual stress
    - Locations of the 4 IFM alignment targets are listed below

Target	X (μm)	Y (μm)
Mass Width Test - 20w-2	2050	1146.75
Mass Width Test - 20w	2050	990.5
Mass Width Test - 52w	2050	830.25
Mass Width Test - 100w	2050	670

- Array of Bistable Mechanisms for Model Validation
    - Optimized for minimal sensitivity to edge bias
    - Expected Force Range: -1 μN to 6 μN
    - These can be tested by using a probe and looking at whether they are bistable or not. The 1p05w device should ALWAYS be bistable (regardless of residual stress or line width variation). The 1p25w device should also always be bistable. The 1p35w device is border-line so it should be about 50-50 unless the residual stress is high, in which case it should always be bistable. The 1p45w device should always be non-bistable, unless the residual stress is high, in which case it should be about 75-25 bistable. The 1p65w device should ALWAYS be NON-bistable. If the residual stress is very high, then there may be a few devices that are bistable, but most likely not.
    - Locations of the IFM alignment targets are listed below

Target	X (μm)	Y (μm)
FCBM Array - 1.65	775	1350
FCBM Array - 1.45	775	1516.25
FCBM Array - 1.35	775	1672.5
FCBM Array - 1.25	775	1838.75
FCBM Array - 1.05	775	1995

A.3 Revision 6 Notes

A.3.1 General Features of the Production Die

- **Top-Down Shadowing**: Should also work for evaporative metallization
- Reason for choosing 250g (J6A) and 2500g (J6B) set points
    - Both devices worked on Revision 4 (performed well in shock tests)
    - The 250g device will allow us to do centrifuge and hammer strike tests
    - The 2500g device has had extensive modeling (J2A – see 2007 report [Mitchell et al. 2008])
    - 250g and 2500g provides a good spread within the medium-g range
- **Redundancy**: Except for a few modules on Revision 3, we don't have any production dice that include redundancy. We will have two of each of the different designs on a single die. The only difference between the two sets of devices on the left side is dimple below the shorting bar.
- Dimple or no dimple: It is unknown whether sputtering will cause the shorting bar end of the mechanism to possibly be "welded" to the substrate (like we saw with Revision 1). We don't think that we need a dimple below the shorting bar, but just in case, we have included the dimple. Revision 4 parts had Dimple 1, but there is still a risk that Dimple 1 could cause problems like those seen in Revision 2.
- Using identical actuators for the Open and Close actuators
- Removed other Dimple 1 guides from edges of mechanisms. The difference in the mass is nearly insignificant, but the added mass on the shorting bar partially offsets the difference anyway.
- J6A-1, J6B-1
    - Includes Dimple 1 below shorting bar
- J6A-2, J6B-2
    - No Dimple 1 below shorting bar
- J6A-3, J6B-3
    - Same as J6X-1 except that Hard Stop has been moved in and other gaps are adjusted
- **Floating the Contacts:** This is our best option for eliminating the *actuator-to-mechanism welding* failure mode. We cannot use nitride for electrical isolation on this Samples run.
- **Removed Dimple Guides:** The 250g and 2500g designs are basically the same devices as the Revision 4 designs, except that the dimple guides on the mechanisms have been removed. This will result in the mass being slightly less, but the difference is almost insignificant. The main purpose for doing this is to make a clear and obvious distinction from the devices that include dimples.

A.3.2 Test Structures

- J6A and J6B with No Poly4 Lid
    - Modal Analysis
    - Mass identical to actual

    - WYKO measurements of Out-Of-Plane Motion
    - Included an alignment feature for the IFM
    - The vernier doesn't add a significant amount of mass
- Measurement of SSP
    - Verniers on ends of bistable mechanisms to measure SSP
- Resonant frequency measurements at FSP and SSP
    - All of the 4 devices can be toggled manually between FSP and SSP and LDV can be used to measure vibration modes.
- Bow-Tie residual stress testers (for Package-Induced stresses, also)
    - P2 and P3 and P2/P3 test devices.
    - These structures are meant to be analyzed using pattern matching, rather than by eye.
- IFM In-Plane force calibration verification
    - Force gauge with k=9.6±1.7 µN/µm (P3+P4)
    - Aligned below IFM alignment target
- Profilometer Test
    - Measure gaps and poly thicknesses
- Weld Test
    - Used to test whether we can get silicon to stick to silicon when a current is run through it
- Sputter Test Structures
    - Cross-over
    - Bond-pad
    - Traces
    - Movable Contacts
    - Actuator-to-trace
    - Poly2, Poly3, and Poly4 shadow distance
    - Actuator push-tab
    - Poly4 etch holes

A.4 Revision 7 Notes

A.4.1 Model Results and Design Parameters

Table A-4. Nominal Quasi-static Analysis Results Using the 2D-Shell Model with a Fine Mesh

Device	Set Point	Mass	S_{max}	F_{max}	$x(F_{max})$	F_{min}	$x(F_{min})$	FSP	UEP	SSP
	g's	mg	MPa	µN	µm	µN	µm	µm	µm	µm
J7A	155	7.262E-04	555.6	20.10	2.23	-1.103	9.37	-0.0010	8.2792	10.3870
J7B	280	4.122E-04	547.6	20.12	2.24	-1.133	9.3896	-0.0010	8.2744	10.4082
J7C	547	3.874E-04	796.0	34.21	1.82	-2.081	8.2247	-0.0009	7.1739	9.1971
J7D	1072	4.851E-04	766.2	86.28	1.78	-5.105	9.1858	-0.0009	7.9322	10.3268
J7E	2549	4.624E-04	946.3	124.93	1.44	-11.572	7.1469	-0.0008	5.9323	8.2183
J7F	5141	2.251E-04	939.4	124.30	1.44	-11.362	7.1421	-0.0008	5.9348	8.2048
J7G	8071	2.755E-04	1302.4	170.09	1.37	-21.836	6.6853	-0.0007	5.3236	7.8577
J7H	10611	2.040E-04	1284.0	168.76	1.39	-21.257	6.6819	-0.0008	5.3379	7.8402
J7K	24967	2.116E-04	881.2	202.02	1.59	-51.883	6.2095	-0.0008	4.5695	7.5901
J7B w8	273	4.167E-04	545.9	20.09	2.24	-1.119	9.3841	-0.0012	8.2758	10.3955
J7B w16	258	4.257E-04	551.4	20.12	2.24	-1.080	9.3758	0.0007	8.2905	10.3696
J7B w32	245	4.436E-04	554.7	20.06	2.24	-1.068	9.375	0.0066	8.2934	10.3653

Note: The devices labeled "J7B w8", "J7B w16", and "J7B w32" represent the variations with the different anchor widths of 8µm, 16µm, and 32µm, respectively.

Table A-5. Revision 7 In-plane Resonant Frequencies Using the SDOF analytical Model and Force-Displacement Curves Generated from the 2Dshell Model at the First Stable Position (FSP) and Second Stable Position (SSP).

	Resonant Frequency	
	FSP	SSP
Device	kHz	kHz
J7A	65.4	16.4
J7B	38.4	10.5
J7C	56.8	18.8
J7D	79.8	20.6
J7E	131.3	34.0
J7F	160.8	49.1
J7G	151.8	59.5
J7H	191.0	68.9
J7K	174.0	99.3

Table A-6. Revision 7 Gaps and Spacing for the Mechanism, Actuators, and Contacts (see Figure 13 and Figure 15).

Device	d_{gap} (um)	d_{latch} (um)	$d_{A\text{-}M}$ (um)	$d_{A\text{-}C}$ (um)	d_{stop} (um)	$x_{contact}$ (um)	x_{stop} (um)
J7A	6.06	8.41	1	2.5	11.8	2.25	12
J7B	6.06	8.41	1	2.5	11.8	2.25	12
J7C	6.31	8.41	2	2.5	10.8	2	11
J7D	6.31	8.41	1.5	3	11.3	2	11.5
J7E	6.81	8.41	2.5	2	9.8	1.5	10
J7F	6.81	8.41	2.5	2	9.8	1.5	10
J7G	6.81	8.41	3	2	8.8	1.5	9
J7H	6.81	8.41	3	2	8.8	1.5	9
J7K	6.81	8.41	2.5	1	8.3	1.5	8.5

Table A-7. Revision 7 Contact and Stop Positions for Mitigation of Vibration Sensitivity (see Figure 13 and Figure 15).

Device	d_{gap} (um)	d_{latch} (um)	$d_{A\text{-}M}$ (um)	$d_{A\text{-}C}$ (um)	d_{stop} (um)	$x_{contact}$ (um)	x_{stop} (um)
J7B	6.06	8.41	1	2.5	11.8	2.25	12.0
J7B HS-1	6.06	8.41	2	2	9.8	2.25	10.0
J7B HS-2	6.06	8.41	1.5	2	10.4	2.25	10.6
J7B HS-3	6.06	8.41	1	2	10.7	2.25	10.9
J7E	6.81	8.41	2.5	2	9.8	1.5	10.0
J7E HS-1	6.81	8.41	3	1	7.6	1.5	7.8
J7E HS-2	6.81	8.41	3	1.7	8.3	1.5	8.5
J7E HS-3	6.81	8.41	3	2	8.6	1.5	8.8

A.4.2 General Features

- *Metallization* – layout for top-down sputter deposition, should also work for evaporation. Test structures on Revision 6 worked, and a few devices were actuated, so we have high confidence that the top-down sputtering will work on Revision 7 as well.
- *Actuators* – Same thermal actuators on both sides of the device. Need to position the close actuator just beyond the hard stop, to minimize the distance required to push the switch closed.
- *Anchor Modification*
    - All devices are designed with the new 4 µm wide anchor.
- *Nitride Isolation*
    - Split the lot at the nitride step (3 wafers). Hold the others at that step until after we've tested the nitride isolation stuff
    - Design with floating contacts so that we don't need to rely on nitride isolation working.
- *Dimples* – The sole reason for considering the use of Dimple 1 on the mechanisms is to prevent the devices from getting stuck to the substrate. This has happened in the past when using Evaporation – the device gets pushed to the substrate and the metal ends up "welding" the device to the substrate (at the shorting bar where the mechanism sticks out from under the Poly 4 lid). It can be subsequently broken free by pushing with a probe.

To avoid this, we have put a dimple on the end of the mechanism to prevent it from touching the substrate. Note that Revision 4 had Dimple 1 and we didn't see the same problems as in Revision 2, which had both Dimple 1 and Dimple 3 (FA showed Dimple 3 to be the likely problem in Revision 2). Further FA of Revision 4 testing showed that the Dimple 1 may have been a cause for failure during temperature cycling.
Update: Testing of 5 dice (10 parts) *without* dimples on Revision 6 showed no "stuck" failures. For this reason, we decided that the baseline parts on Revision 7 will have no dimples on the mechanism, but we will include two dice *with* dimples, just in case. *One possibility would be to make the Dimple 1 shorter by modifying the process.* But, if we do that, and all the devices work, we won't know whether using the original height Dimple 1 would have been okay or not.

- *Frequency Content*
    - Use of hard stop to reduce sensitivity to vibration, but this may cause problems with dormancy, and adhesion may affect the set point. Revision 6 has 2 devices (250g, 2500g) but we won't be able to test these before Revision 7 submission. Two die have been included containing 4 copies of a single device (4×250g and 4×2500g). In each case, the hard stops are placed in 4 different locations. The first is the default location (well away from the SSP), the 2nd is a conservative distance from the SSP, and the 3rd is a more aggressive distance from the SSP but still hopefully not in constant contact. The 4th is designed to be in constant contact (like the Revision 6 designs).
    - Design a couple devices with high steady-state set points so that in the presence of high freq content, it closes at, say, 2000 g. We designed a new 5g-k, 7.5k-g, and 10k-g and have a 25k-g in two of the singlet die.
- *Temperature Effects*
    - Array of mechanisms with different anchor sizes to determine effect of cold temperature
    - 4 copies of the 250g design were included on a single die, with different anchor widths. These can be wired up, allowing the devices to be tested inside the package. A slight change in the quasi-static threshold is expected due to the change in the geometry of the frame. We expect to perform thermal testing in which we gradually lower the temperature of the chamber and see when (at what temperature) each of the devices close.
- Design for *Packaging*
    - Included a dicing map and labeled the modules according to this map
    - Included fiducials from Revision 6.

A.4.3 Die-Specific Information

The modules have been labeled according to the traditional Dicing Map scheme (modules are labeled 1 through 8 when the reticle is rotated by 90 degrees).

- Die **6B** : The default die: 150g, 250g, 500g, 1000g, no Dimple 1
- Die **6A** : The default die: 2500g, 5000g, 7500g, 10000g, no Dimple 1
- Die **7B** : Same as 6B except that Dimple 1 has been added to the mechanism
- Die **7A** : Same as 6A except that Dimple 1 has been added to the mechanism

- Die **8B** : 4 copies of the 250g device each with a different hard stop location, including the default device.
- Die **8A** : 4 copies of the 2500g device each with a different hard stop location, including the default device.
- Die **2B** : 2500g – 4 Devices in all different directions for bi-axial/bi-directional array
- Die **2A :** 250g – 4 Devices in all different directions for bi-axial/bi-directional array
- Die **3B** : 4 copies of the default 2500g device for testing the variation from device-to-device within a single package
- Die **3A** : Model validation via centrifuge testing. 2 copies of the default 150g device and 2 copies of the default 250g device. The 2 copies of each will provide some device-to-device variation data. Both devices use the same spring design; the difference is only the size of the mass. A thickness measurement device is included to aid in model validation. Edge bias could be measured by looking at the contact spring prior to metallization. Residual stress is measured using the bowtie structure.
- Die **4A** : Anchor Width Test. 4 Copies of the 250g device with different anchor widths: 4µm (the default), 8µm, 16µm, and 32µm.
- Die **4B** : The test structure module
- Die **1A-1H** : Singlets (~1.5×1.5mm die). 2 × 25kg, 2 × 10kg, 2 × 7.5kg, 2 × 5 kg. Copies include 1 with and 1 without Dimple 1 under the contact bar.
- Die **5A-5H** : Singlets (~1.5×1.5mm die). 2 × 2.5kg, 2 × 1.0kg, 2 × 500g, 1 × 250g, 1 × 150g. Copies include 1 with and 1 without Dimple 1 under the contact bar. Default is without Dimple 1.

A.4.4 Test Structures

See Figure A-4 for the Revision 7 test structure module.

- Nitride Isolation
    - Pull-tab tests, modified from previous versions, to test the fracture strength of the nitride via (different lengths and numbers of vias)
    - Electrical tests for comparing the resistance of poly-to-poly (sacox3 cut) and the nitride isolation. These structures can also be used to test the breakdown voltage.
- Si-Si Welding tester
    - Parallel spring connected to push spring so that you push the contacts closed then run a current through them to see if the contact will remain stuck together. You can get a rough idea of the force by looking at the spring compression.
    - With and without nitride isolation
- Resonant frequency measurements at FSP and SSP
    - All of the 4 devices can be toggled manually between FSP and SSP and LDV can be used to measure vibration modes.
    - The J7A and J7F devices have versions with and without the lid, to compare the quality factors.
    - These devices can also be used for modal analysis and IFM force-displacement measurements.

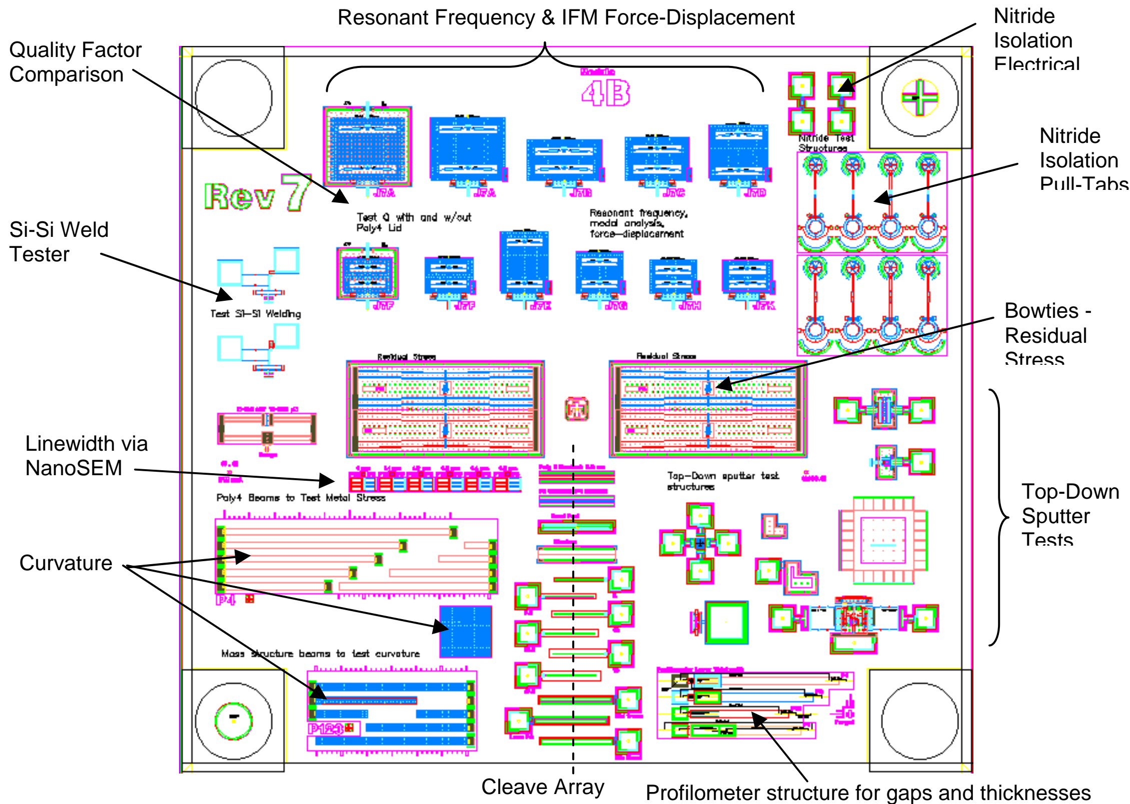

Figure A-4. Revision 7 test structure module.

- Bow-Tie residual stress testers (for package-induced stresses, also)
  - P2 and P3 test devices on every die. The test structure die has the P2 and P3 along the same axis as the devices.
  - These structures are meant to be analyzed using pattern matching, rather than by eye.
  - A spreadsheet is available for calculating stress vs. displacement.
- Width measurement device
  - Poly12 and Poly3 beams with roughly the same dimensions as the springs
- Poly 4 beams (fixed-fixed and cantilever) to test metal stress and curvature via interferometry. Test the beams before and after metallization.
- Profilometer test structure for measuring poly thicknesses, dimple gaps, and oxide gaps. This structure is slated to be added to the standard SUMMiT V frame.
- Curvature due to Residual Stress (initially on Revision 5)
  - Include non-lidded structures for looking at under WYKO
  - Compare curvature of mushroom vs. beam with same mass structure
- IFM In-Plane force calibration verification
  - Force gauge with k=9.6±1.7 μN/μm (P3+P4)
  - Aligned below IFM alignment target
- Sputter Test Structures
  - Cross-over
  - Bond-pad
  - Traces

- Movable Contacts
- Actuator-to-trace
- Array of beams for cleaving/SEM
  - Poly2 shadow distance
  - Bond pads
  - traces
- Actuator push-tab
- Poly4 etch holes

Appendix B:
SCBM ANSYS Model

B.1 M-file used to store the input parameters for the Revision 7 1F bistable mechanism

```
% Input Parameters used for the SCBM Ansys Model
%
% Units: um, uN, mg, ms, MPa
% density in mg/um^3 or kg/m^3 * 1e-12
% velocity in mm/s or um/ms
% acceleration in um/ms^2 or m/s^2
% power in nW
% frequency in mrad/s or rad/ms or rad/s * 1e3 or cycles/ms

%% GEOMETRY

geom.edgeBias= -0.1;

% GEOMETRY of SPRINGS
% The J4A spring geometry was based on the Run19 from the Design Space
% Study (dev_Jseries_Run19) and modified to be a 2f spring. The 1f spring
% is a slight modification of the 2f spring
geom.l13= 26;
geom.a13= 8.5;
geom.w13= 1.02;
geom.l2= 65;
geom.a2= 1.525;

geom.l2b= -4;
geom.w2ac= 6.2;
geom.w2b= 2.2;
geom.thickA= 2.25;
geom.thickB= 2.2;
geom.thickC= 2.25;

% GEOMETRY of MASS
geom.totalMass= 4.0e-4;     % Not important for quasi-static analysis
geom.anchXLen= 4;
geom.massCutoutY=36;
geom.massEndWidth=28;   % 12, 20, 28,...
geom.massSideWidth=28;  % 12, 20, 28,...
geom.massMidWidth=28;   % 12, 20, 28,...
% ... for Beam Model
geom.beamElemLen = 1;   % Length of beam elements
% ... for 2Dshell Model
geom.massElemWidth=12;
geom.massElemPitch=8;
geom.massElemHole=1.2;
geom.plateElemNum= 2;  % Number of elements in Plate
```

```
geom.nemw= 6;  % Number of elements across beam
geom.nemr= 12; % Number of elements across the semi-rigid segment

%% MATERIALS
mat.ymod= 164000;
mat.prat= 0.2300;
mat.rstress= -8.5000;
mat.density= 2.33e-009;
mat.cteC0= 2.3267e-006;
mat.cteC1= 9.8409e-009;
mat.cteC2= -2.8553e-011;
mat.cteC3= 5.0993e-014;
mat.cteC4= -3.8958e-017;

%% LOADS
loads.staticLoadSteps= 30;
loads.yDist= 12.5;
loads.tempRef= 22;
loads.tempApplied= 22;

loads.calcZStiff= 1;
loads.xDist= 0;
loads.zDist= 0;
loads.uxLR= 0;
loads.uxUR= 0;
loads.uxUL= 0;
loads.uyLR= 0;
loads.uyUL= 0;
loads.uyUR= 0;
loads.gXStatic= 0;
loads.gYStatic= 0;
loads.gZStatic= 0;
```

B.2 Setting up the Dynamic Model

1. Run the `reverseforce.m` Matlab function. You will be asked to select a force-displacement results file (such as `J7D_shock_static_results_nom.txt`). The function analyzes the force displacement curve, reverses the curve so that x=0 corresponds to the device starting at the second stable position (with positive motion defined as motion towards the first stable position). The function prompts you to save two files – one for the forward curve (starting at the FSP) and one for the reverse curve (starting at the SSP). The resulting files will consist of two columns [displacement force], and the function extrapolates to extend the force displacement curve (for purely mathematical purposes related to how the dynamic model converges).
2. Save the resulting force-displacement data files in the fd_tables directory.
3. Create an `inputs_RevX_XXX.m` file for each of the devices, using the nominal values reported in Table 2, Table 3, and Table 4.
4. Run `solve_fcbm_freq_at_SSP.m` for each set of inputs to evaluate the resonant frequency at the SSP and FSP. Record these values in the inputs file (they are used to create lines on plots in other simulations)

Distribution

4 MS1064 John A. Mitchell, 2614

Electronic Distribution:

1 MS0340 John L. Sichler, 2123 (electronic copy)
1 MS0340 Steve Harris, 2123 (electronic copy)
1 MS0343 Mary E. Gonzales, 2120 (electronic copy)
1 MS0343 Anna L. Schauer, 2610 (electronic copy)
1 MS0344 George Clark, 2626 (electronic copy)
1 MS0372 James M. Redmond, 1525 (electronic copy)
1 MS0421 Michael R. Sjulin, 0240 (electronic copy)
1 MS0427 Robert A. Paulsen, 2011 (electronic copy)
1 MS0447 Matt Kerschen, 2111 (electronic copy)
1 MS0530 Hae-Jung L. Murphy, 2623 (electronic copy)
1 MS0633 Todd Sterk, 2952 (electronic copy)
1 MS0821 Anthony Thornton, 1530 (electronic copy)
1 MS0824 Tze Y. Chu, 1500 (electronic copy)
1 MS0847 Peter J. Wilson, 1520 (electronic copy)
1 MS1064 Joel B. Wirth, 2614 (electronic copy)
1 MS1064 Rebecca C. Clemens, 2614 (electronic copy)
1 MS1064 Ernest J. Garcia, 2614 (electronic copy)
1 MS1064 Marc A. Polosky, 2614 (electronic copy)
1 MS1069 Mark R. Platzbecker, 1749-1 (electronic copy)
1 MS1069 Michael S. Baker, 1749-1 (electronic copy)
1 MS1069 Danelle M. Tanner, 1749-1 (electronic copy)
1 MS1069 Jonathan W. Wittwer, 1749-1 (electronic copy)
1 MS1070 Channy C. Wong, 1526 (electronic copy)
1 MS1070 Jill Blecke, 1526 (electronic copy)
1 MS1070 David S. Epp, 1526 (electronic copy)
1 MS1080 Keith Ortiz, 1749 (electronic copy)
1 MS1081 David J. Stein, 1726 (electronic copy)
1 MS1081 Jeremy A. Walraven, 1726 (electronic copy)
1 MS1160 Douglas A. Dederman, 5431 (electronic copy)
1 MS1415 David R. Sandison, 1110 (electronic copy)
1 MS1415 Carlos Gutierrez, 1114 (electronic copy)
1 MS1415 Douglas A. Crowson, 1114 (electronic copy)
1 MS1415 Jack E. Houston, 1114 (electronic copy)
1 MS9042 Davina M. Kwon, 8770 (electronic copy)
1 MS9102 James F. Stamps, 8235 (electronic copy)
1 MS9102 Paul Y. Yoon, 8235 (electronic copy)
1 MS9153 Russell G. Miller, 8240 (electronic copy)
1 MS9154 Janson Wu, 8244 (electronic copy)
1 MS9154 Jennifer Chan, 8244 (electronic copy)
1 MS9154 Judy Lau, 8244 (electronic copy)
1 MS0899 Technical Library, 9536 (electronic copy)

Sandia National Laboratories